

## Order- $\alpha_s^2$ QCD corrections to the reaction $p + \bar{p} \rightarrow W^+ + \gamma + X$ in the soft-plus-virtual-gluon approximation

S. Mendoza and J. Smith

*Institute for Theoretical Physics, State University of New York at Stony Brook, Stony Brook, New York 11794-3840*

W. L. van Neerven

*Instituut Lorentz, University of Leiden, P.O. Box 9506, 2300 RA Leiden, South Holland, The Netherlands*

(Received 17 December 1992)

We examine the sensitivity of the total cross section and inclusive photon distributions for the reaction  $p + \bar{p} \rightarrow W^+ + \gamma + X$  to changes in the QCD renormalization scale, mass factorization scale, and mass factorization scheme in  $O(\alpha_s)$ . Based on these findings, a higher-order- $\alpha_s$  approximation prescription is proposed and, by readjusting the QCD mass factorization and renormalization scales,  $O(\alpha_s^2)$  predictions are obtained for the reaction cross sections and inclusive photon distributions for the CERN Super Proton Synchrotron (SppS) ( $\sqrt{S} = 0.63$  TeV) and Fermilab Tevatron ( $\sqrt{S} = 1.8$  TeV) colliders.

PACS number(s): 13.85.Qk, 12.38.Bx, 14.80.Er

### I. INTRODUCTION

The calculation of many  $O(\alpha_s)$  QCD [1] corrections to inclusive and semi-inclusive processes have now been completed. For some particular cases it has been possible to extend these calculations to find exact results beyond the lowest order of  $\alpha_s$ . An example of the latter is the quantity  $R$  defined in the reaction  $e^+ + e^- \rightarrow X$ , where  $X$  is any hadronic state, which is now completely known up to order  $\alpha_s^3$  [2]. Further, we want to mention the  $O(\alpha_s^2)$  correction to the two-jet cross section for the same process [3] and the  $O(\alpha_s^2)$  correction to the Drell-Yan (DY)  $K$  factor which has been computed in both the modified minimal subtraction ( $\overline{\text{MS}}$ ) [4] and the deep-inelastic scattering (DIS) schemes [5].

The results of these calculations show that the size of the corrections can be rather large, a feature which in many cases can be primarily attributed to the soft-plus-virtual-gluon contributions. Even though the expressions for the corrections can be very complicated, which is generally the case when the Born cross section is already of order  $\alpha_s$  or higher, it usually turns out that the  $O(\alpha_s)$ -corrected distributions only differ slightly in shape from the lowest-order ones. This indicates that the theoretical  $K$  factor is only a slowly varying function of the kinematical variables in the reaction, such as the transverse momenta or rapidities. Essentially, the (differential) cross sections for the  $O(\alpha_s)$ -corrected process are proportional to those of the uncorrected process. Examples are direct photon production  $p + \bar{p} \rightarrow \gamma + X$  [6], heavy flavor production  $p + \bar{p} \rightarrow Q + \bar{Q} + X$  [7,8], and radiative  $W$  production  $p + \bar{p} \rightarrow W^+ + \gamma + X$  [9,10]. The intricacy as well as the behavior of the  $O(\alpha_s)$  corrections have inspired some authors to construct approximate formulas for various types of processes using renormalization-group methods. In particular, this approach was very successful for the reaction  $p + \bar{p} \rightarrow W^+ + \gamma + X$  [10] due to its close resemblance to the DY reaction  $p + \bar{p} \rightarrow W + X$ . Both reactions proceed mainly via the quark-antiquark ( $q\bar{q}$ ) subprocess

which is dominated by the soft-plus-virtual-gluon radiation contributions at small c.m. energies. At the CERN Super Proton Synchrotron (SppS) collider ( $\sqrt{S} = 0.63$  TeV) the latter contributions are sufficient to describe the cross section and inclusive photon distributions in the reaction  $p + \bar{p} \rightarrow W + \gamma + X$ . However, at larger energies (e.g., at the Fermilab Tevatron) the soft-plus-virtual-gluon approximation is not so good. This is caused by the increasing contributions from both the hard-gluon radiation in the  $q\bar{q}$  channel and from the parton subprocesses  $g + q(\bar{q}) \rightarrow W + \gamma + q(\bar{q})$ . Even though these pieces partially cancel each other the remainder is not negligible. For this reason we want to give a better approximation to the  $O(\alpha_s)$  soft-plus-virtual cross section which compensates for the latter contributions. Note here that one can construct analogous compensating pieces in the soft-plus-virtual approximation to the DY reaction where it is known that there is a partial cancellation between the missing hard-gluon radiation and contributions from the gluon-quark ( $gq$ ) and gluon-antiquark ( $g\bar{q}$ ) subprocesses. This is accomplished by a readjustment of the mass factorization and renormalization scales in the soft-plus-virtual-gluon approximation as will be explained more fully later. In addition we want to include the dominant  $O(\alpha_s^2)$  corrections from the soft-plus-virtual contributions at this readjusted scale in order to give an estimate of the cross section beyond the first order in  $\alpha_s$ .

The reason for studying the process  $p + \bar{p} \rightarrow W + \gamma + X$  is due to the discovery of a zero in the amplitude of the parton-parton subprocess  $q + \bar{q} \rightarrow W + \gamma$  [11]. This phenomenon gives one hope that properties of the magnetic moment and quadrupole moment of the  $W$  boson might be measurable [12]. A general discussion of non-standard electromagnetic couplings of the charged  $W$  boson has been given recently [13]. The latest experimental results are given in [14] and [15]. In our work we assume the validity of the standard model. The  $O(\alpha_s)$  QCD corrections due to final-state gluon radiation in the reac-

tion  $q + \bar{q} \rightarrow W^+ + \gamma + X$  including the virtual contributions have been calculated in [9]. The analogous calculation for the initial-state gluon radiation was given in [10], where we gave complete results for the QCD corrections to  $p + \bar{p} \rightarrow W^+ + \gamma + X$  in the DIS mass factorization scheme. Notice that we also included the contributions from the  $gq$  and  $g\bar{q}$  subprocesses. Here we shall primarily concentrate on getting an estimate of the  $O(\alpha_s^2)$  contribution which can be made from an approximation containing the dominant initial-state gluon radiation. The properties of the  $K$  factor mentioned above are also valid here.

Our paper will be organized as follows. In Sec. II we will present the exact formulas for the  $O(\alpha_s)$  corrections to the process  $p + \bar{p} \rightarrow W^+ + \gamma + X$  in both the DIS and  $\overline{\text{MS}}$  mass factorization schemes, showing the explicit dependence on the renormalization and mass factorization scales  $R$  and  $M$ , respectively. In Sec. III we will discuss two higher-order approximations and show how to obtain an approximate formula for the  $O(\alpha_s^2)$  corrections. Since the actual expressions for the latter are rather long we have put them in Appendixes A and B. In Sec. IV we will study the choice of scales and scheme at  $O(\alpha_s)$  and, by comparing the approximate with the exact results at  $O(\alpha_s)$ , will justify which is the better approximation. Then we will present our results from the  $O(\alpha_s^2)$  approximation. This will be done by examining both the total cross sections and inclusive photon differential distributions after inclusion of the modifications necessary to give a correct definition for  $\alpha_s$  and the incorporation of the latest parton densities.

## II. EXACT FIRST-ORDER CORRECTIONS IN THE DIS AND $\overline{\text{MS}}$ SCHEMES

The reaction under consideration is given by

$$p + \bar{p} \rightarrow W^+ + \gamma + X, \quad (2.1)$$

where  $X$  denotes any final hadronic state. In lowest-order perturbation theory the only parton subprocess contributing to the above reaction is given by the quark-antiquark annihilation process:

$$q(p_1) + \bar{q}(p_2) \rightarrow W^+(q) + \gamma(k), \quad (2.2)$$

where the particle momenta are given in parentheses. The three graphs which contribute to the Born amplitude for the reaction are shown in Fig. 1 of [10], and, like the lowest-order Drell-Yan process, do not contain the QCD coupling constant. The charges of the quarks  $q(p_1), \bar{q}(p_2)$  are  $Q_1$  and  $Q_2$ , respectively (all in units of the electric charge), while  $Q = Q_1 - Q_2$  is the  $W$ -boson charge. The weak-coupling constant will be denoted by  $g/2\sqrt{2}$  which can also be written as  $g = 2M_W(\sqrt{2}G_F)^{1/2} = e/\sin\theta_W$ . Here  $G_F$  and  $\theta_W$  denote the Fermi constant and the weak mixing angle, respectively. For the kinematical variables we choose

$$s = 2p_1 \cdot p_2, \quad t = -2k \cdot p_1, \quad u = -2k \cdot p_2. \quad (2.3)$$

Since we work with massless quarks, the invariants are related at the Born level by  $s + t + u = s_4 = M_W^2$ . The Born cross section for process (2.2) is given by

$$s^2 \frac{d\hat{\sigma}_{q\bar{q}}^{(0)}}{dt du} = \delta(s_4 - M_W^2) B_{\text{QED}}(s, t, u, M_W^2), \quad (2.4)$$

where

$$B_{\text{QED}}(s, t, u, M_W^2) = \frac{1}{12} \alpha g^2 \frac{(Q_1 u + Q_2 t)^2}{ut(s - M_W^2)^2} [sM_W^2 + \frac{1}{2}(u^2 + t^2)]. \quad (2.5)$$

Here we have averaged over the initial quark spins and colors and summed over the final polarization states of the  $W$  boson and the photon. The radiation zero now reveals itself when  $Q_1 u + Q_2 t = 0$  where the differential cross section in (2.4) vanishes.

The  $O(\alpha_s)$ -corrected cross section of reaction (2.1) is obtained from the virtual corrections to process (2.2) and the gluon bremsstrahlung process:

$$q(p_1) + \bar{q}(p_2) \rightarrow W^+(q) + \gamma(k) + g(k'). \quad (2.6)$$

Here we distinguish between soft ( $s_4 < M_W^2 + \Delta$ ) and hard ( $s_4 > M_W^2 + \Delta$ ) gluons so that the cross section will be split into a soft and a hard part [10]. After adding the two pieces all dependence upon  $\Delta$  vanishes. We have also taken into consideration the gluon (anti)quark reactions

$$\begin{aligned} q(p_1) + g(p_2) &\rightarrow W^+(q) + \gamma(k) + q(k'), \\ g(p_1) + \bar{q}(p_2) &\rightarrow W^+(q) + \gamma(k) + \bar{q}(k'). \end{aligned} \quad (2.7)$$

The exact expressions for the cross sections of the processes in (2.6) and (2.7) were given in Ref. [10]. They were presented in the DIS scheme as well as in the DY scheme (in Ref. [10] these schemes were called  $C$  and  $D$ , respectively.) In the DIS scheme the nonpole term of the transition function is determined in such a way that the deep-inelastic Wilson coefficient corresponding to the deep-inelastic structure function  $F_2(x, Q^2)$  does not receive corrections in any order of  $\alpha_s$ . The same applies to the DY scheme in which the DY cross section has no corrections. Notice that the pole terms<sup>1</sup> in the transition functions stand for the collinear divergences which have to be removed from the renormalized (in this case only with respect to coupling-constant renormalization) parton cross section. In the literature, several parametrizations for the parton densities are available. Here we prefer to use the recent Morfin-Tung parametrization [16] for the parton densities since they are available in both the DIS scheme as well as the  $\overline{\text{MS}}$  scheme. Notice that in [10] we used the DIS parametrization in [17]. The DY scheme is a purely theoretical scheme because there are no measured parton densities in that scheme. We have only used the latter to facilitate the discussion following below. The relation between the parton cross sections determined in the DY scheme ( $D$ ) and in the DIS scheme ( $C$ ) is given by

<sup>1</sup>The residue of the pole terms in the transition function are represented by the Altarelli-Parisi splitting functions.

$$\left[ s^2 \frac{d^2 \hat{\sigma}_{ij}(s, t, u, R^2, M^2)}{dt du} \right]^C = \int_0^1 \frac{dx_1}{x_1} \int_0^1 \frac{dx_2}{x_2} \Gamma_{li}^{DC}(x_1, \kappa^2, R^2, M^2) \Gamma_{mj}^{DC}(x_2, \kappa^2, R^2, M^2) \left[ \hat{s}^2 \frac{d^2 \hat{\sigma}_{lm}(\hat{s}, \hat{t}, \hat{u}, \kappa^2)}{d\hat{t} d\hat{u}} \right]^D, \quad (2.8)$$

where  $\hat{s} = x_1 x_2 s$ ,  $\hat{t} = x_1 t$ , and  $\hat{u} = x_2 u$ . The parameter  $\kappa^2$  appearing in the cross section  $(d\hat{\sigma}_{lm})^D$  on the right-hand side of (2.8) stands for the mass factorization scale. In [10] we chose it to be equal to the renormalization scale and set  $\kappa^2 = s$ . The parameters  $R$  and  $M$  which appear in the transition functions  $\Gamma_{ij}^{DC}$  and in the cross sections  $(d\hat{\sigma}_{ij})^C$  denote the renormalization and mass factorization scales in the  $C$  scheme, respectively.

Note that the above transition functions  $\Gamma_{li}^{DC}$  can be inferred from the DY cross section, provided it is calculated in the DIS scheme. This latter cross section can be denoted by

$$\frac{d\sigma}{dQ^2} = \tau \sigma_W(Q^2, M_W^2) W(\tau, Q^2), \quad \tau = \frac{Q^2}{S}, \quad (2.9)$$

where  $\sigma_W$  is the pointlike DY cross section for  $W$  production,  $\sqrt{S}$  is the c.m. energy of the incoming hadrons, and  $\sqrt{Q^2}$  is the invariant mass of the leptons into which the  $W$  boson decays. The total cross section follows from (2.9) by using the narrow-width approximation. According to the DY mechanism the hadronic structure function  $W(\tau, Q^2)$  can be written as

$$W(\tau, Q^2) = \sum_{ij} \int_0^1 dx_1 \int_0^1 dx_2 \int_0^1 dx_3 \delta(\tau - x_1 x_2 x_3) D_{Pij}(x_1, x_2, R^2, M^2) \Delta_{ij}(x_3, Q^2, R^2, M^2). \quad (2.10)$$

Here  $D_{Pij}(x_1, x_2, R^2, M^2)$  is the usual combination of parton densities. The Wilson coefficient  $\Delta_{ij}(x, Q^2, R^2, M^2)$  stands for the QCD correction term to the zeroth order process, which is known up to  $O(\alpha_s^2)$  in the  $\overline{\text{MS}}$  [4] as well as the DIS schemes [5]. The transition functions  $\Gamma_{li}^{DC}$ , bringing us from the DY scheme to the DIS scheme, can now be derived from

$$\Delta_{ij}^C(x, Q^2, R^2, M^2) = \int_0^1 dx_1 \int_0^1 dx_2 \int_0^1 dx_3 \delta(x - x_1 x_2 x_3) \Gamma_{qi}^{DC}(x_1, Q^2, R^2, M^2) \Gamma_{qj}^{DC}(x_2, Q^2, R^2, M^2) \Delta_{q\bar{q}}^D(x_3, Q^2, Q^2, Q^2), \quad (2.11)$$

where

$$\Delta_{q\bar{q}}^D(x_3, Q^2, Q^2, Q^2) = \delta(1 - x_3). \quad (2.12)$$

For completeness we collect the transition functions  $\Gamma_{qi}^{DC} = \Gamma_{q\bar{i}}^{DC}$  up to  $O(\alpha_s)$  in Appendix A.

To this order, the transition functions have the form

$$\begin{aligned} \Gamma_{ij}^{DC}(x, \kappa^2, R^2, M^2) \\ = \delta_{ij} \delta(1 - x) + \frac{\alpha_s(\kappa^2)}{2\pi} [f_{ij}^D(x, \kappa^2, \kappa^2) - f_{ij}^C(x, M^2, \kappa^2)], \end{aligned} \quad (2.13)$$

where  $\alpha_s(\kappa^2)$  has to be replaced by<sup>2</sup>

$$\alpha_s(\kappa^2) = \alpha_s(R^2) \left[ 1 + \frac{\alpha_s(R^2)}{4\pi} \beta_0 \ln \frac{R^2}{\kappa^2} + \dots \right]. \quad (2.14)$$

The constant  $\beta_0$  is the lowest-order coefficient of the  $\beta$  function and equals  $11C_A/3 - 2n_f/3$  with  $C_A = N$  for  $\text{SU}(N)$ . Note that the  $\Gamma_{ij}^{DC}$  as well as the  $d\hat{\sigma}_{ij}$  are finite.

The functions  $f_{ij}$  can be written in any scheme (here  $f_{ij}^C$  or  $f_{ij}^D$ ) as

$$f_{ij}(x, M^2, \kappa^2) = f_{ij}^B(x, M^2, \kappa^2) + \bar{f}_{ij}(x), \quad (2.15)$$

where  $f_{ij}^B(x, M^2, \kappa^2)$  is presented in the  $\overline{\text{MS}}$  scheme (called the  $B$  scheme in [10]). The latter is given by

$$f_{ij}^B(x, M^2, \kappa^2) = P_{ij}^{(0)}(x) \left[ \gamma_E - \ln 4\pi + \ln \frac{M^2}{\kappa^2} \right]. \quad (2.16)$$

Here  $P_{ij}^{(0)}(x)$  denote the lowest-order Altarelli-Parisi (AP) splitting functions. The functions  $\bar{f}_{ij}(x)$  depend on the chosen scheme differing from the  $\overline{\text{MS}}(B)$  one, which implies that  $\bar{f}_{ij}^B = 0$ . For the schemes discussed in this paper, i.e.,  $C$  or  $D$ , they can be found in [18–20]. For completeness we give the definitions of  $f_{qq}(x)$  as used in [10]: namely,

$$\begin{aligned} \bar{f}_{qq}^D(x) &= \bar{f}_{q\bar{q}}^D(x) \\ &= C_F \left[ \left[ \frac{1+x^2}{1-x} \ln \frac{(1-x)^2}{x} \right] \theta(1-x-\delta) \right. \\ &\quad \left. + \delta(1-x) [2 \ln^2 \delta - 4 + 2\zeta(2)] \right], \end{aligned} \quad (2.17)$$

$$\begin{aligned} \bar{f}_{qq}^C(x) &= \bar{f}_{q\bar{q}}^C(x) \\ &= C_F \left\{ \left[ \frac{1+x^2}{1-x} \left[ \ln \frac{1-x}{x} - \frac{3}{4} \right] \right. \right. \\ &\quad \left. \left. + \frac{9}{4} + \frac{5}{4} x \right] \theta(1-x-\delta) \right. \\ &\quad \left. + \delta(1-x) \left[ \ln^2 \delta - \frac{3}{2} \ln \delta - \frac{9}{2} - 2\zeta(2) \right] \right\}, \end{aligned} \quad (2.18)$$

with  $\zeta(2) = \pi^2/6$  and  $\delta$  is a cutoff which separates the

<sup>2</sup>In [10]  $\kappa^2$  was called  $Q^2$ .

soft-gluon region  $1-\delta < x < 1$  from the hard-gluon one  $x < 1-\delta$ . The relationship between the dimensionless  $\delta$  and the  $\Delta$  mentioned after (2.6) has been presented in [10]. In the gluon-quark channel, however, the expressions for the  $f_{qg}(x)$  in [10] should be changed to

$$\begin{aligned} \bar{f}_{qg}^D(x) &= \bar{f}_{qg}^D(x) \\ &= T_f \left[ [x^2 + (1-x)^2] \ln \frac{(1-x)^2}{x} \right. \\ &\quad \left. + \frac{1}{2}(1-x)(1+7x) \right], \end{aligned} \quad (2.19)$$

while

$$\begin{aligned} \left[ s^2 \frac{d^2 \hat{\sigma}_{q\bar{q}}^{(1)}}{dt du} \right]^C &= \left[ s^2 \frac{d^2 \hat{\sigma}_{q\bar{q}}^{(1)}}{dt du} \right]^D \Big|_{\kappa^2=s} \\ &+ \frac{1}{48} \alpha g^2 \frac{\alpha_s(R^2)}{\pi} C_F \left\{ \left[ [Q_1(s+t)u + Q_2(M_W^2 - u)t]^2 [u^2(s+t)^2 + t^2(M_W^2 - u)^2 + 2sM_W^2(M_W^2 - u)(s+t)] \right] \right. \\ &\quad \times \left[ [(s+t)^2 + (M_W^2 - u)^2] \left[ \ln \frac{s_4 - M_W^2}{s+t} + \ln \frac{s}{M^2} + \frac{3}{4} \right] \right. \\ &\quad \left. \left. - \frac{1}{4}(s_4 - M_W^2)[9(s+t) + 5(M_W^2 - u)] \right] \right. \\ &\quad \times u^{-1} t^{-1} (s+t)^{-2} (M_W^2 - u)^{-2} (tM_W^2 + su)^{-2} (s_4 - M_W^2)^{-1} \theta \left[ \frac{s_4 - M_W^2 - \Delta}{s+t} \right] \\ &\quad \left. + (t \leftrightarrow u, Q_1 \leftrightarrow Q_2) \right\} \\ &+ \frac{1}{2} \frac{\alpha_s(R^2)}{\pi} C_F \left\{ \delta(s_4 - M_W^2) B_{\text{QED}}(s, t, u, M_W^2) \right. \\ &\quad \times \left[ \left[ 2 \ln \frac{\Delta}{s+t} + \frac{3}{2} \right] \ln \frac{s}{M^2} + \ln^2 \frac{\Delta}{s+t} + \frac{3}{2} \ln \frac{\Delta}{s+t} + 4\zeta(2) + \frac{1}{2} \right] + (t \leftrightarrow u, Q_1 \leftrightarrow Q_2) \left. \right\}. \end{aligned} \quad (2.21)$$

In a similar way the expression for the quark-gluon process can be obtained and reads as

$$\begin{aligned} \left[ s^2 \frac{d^2 \hat{\sigma}_{qg}}{dt du} \right]^C &= \left[ s^2 \frac{d^2 \hat{\sigma}_{qg}}{dt du} \right]^D \Big|_{\kappa^2=s} \\ &+ \frac{1}{48} \alpha g^2 \frac{\alpha_s(R^2)}{\pi} T_f \left[ [Q_1(M_W^2 - t)u + Q_2(s+u)t]^2 [t^2(s+u)^2 + u^2(M_W^2 - t)^2 + 2sM_W^2(M_W^2 - t)(s+u)] \right. \\ &\quad \times \left\{ [(s+u)^2 - 2(M_W^2 - t)(s+u) + 2(M_W^2 - t)^2] \left[ \ln \frac{s_4 - M_W^2}{s+u} + \ln \frac{s}{M^2} + 1 \right] \right. \\ &\quad \left. \left. + \frac{1}{2}(s_4 - M_W^2)(s+u + 5t - 5M_W^2) \right\} \right. \\ &\quad \times u^{-1} t^{-1} (s+u)^{-3} (M_W^2 - t)^{-2} (M_W^2 u + st)^{-2} \\ &\quad + \frac{1}{48} \alpha g^2 \frac{\alpha_s(R^2)}{\pi} T_f \left[ Q_2^2 [(M_W^2 - s)^2 u^2 + (t+u)^2 s^2 + 2tM_W^2(t+u)(M_W^2 - s)] \right. \\ &\quad \left. \times [(t+u)^2 - 2(M_W^2 - s)(t+u) + 2(M_W^2 - s)^2] \ln \left[ \frac{s}{M^2} \right] \right] \\ &\quad \times s^{-1} u^{-1} (t+u)^{-3} (M_W^2 - s)^{-2}. \end{aligned} \quad (2.22)$$

$$\begin{aligned} \bar{f}_{qg}^C(x) &= \bar{f}_{qg}^C(x) \\ &= T_f \left[ [x^2 + (1-x)^2] \ln \frac{1-x}{x} \right. \\ &\quad \left. + 8x(1-x) - 1 \right], \end{aligned} \quad (2.20)$$

if one averages over the gluon polarization in  $n$  dimensions rather than four. In QCD the color factors  $C_F$  and  $T_f$  are given by  $4/3$  and  $1/2$ , respectively.

From (2.8) and the above results one can determine the  $O(\alpha_s)$  expression for process (2.6) which is

Here the last term, which is proportional to  $Q_2^2$ , is due to quark fragmentation into a photon. This part of the cross section is always given in the  $\overline{\text{MS}}$  scheme. The expression for the gluon-antiquark reaction, i.e.,  $d\sigma_{\bar{q}g}$ , can be obtained from (2.22) by interchanging  $t$  with  $u$  and  $Q_1$  with  $Q_2$ . The above cross sections can also be found in (7.17) and (7.19) of [10] except for the mass factorization term  $\ln s/M^2$  which we have included here.<sup>3</sup> The expressions for  $d\sigma^D$  are extremely long and could not be fully presented in Ref. [10] [see however Eqs. (6.19) and (6.20) for  $q\bar{q}$  and (6.33)<sup>4</sup> for  $qg$ ].  $d\sigma^D$  in these formulas must be evaluated at a mass factorization scale  $\kappa=\sqrt{s}$ , and a renormalization scale  $\mu=R$ . The complete expressions are in our computer program and can be obtained upon request. Since the parton densities are also parametrized in the  $\overline{\text{MS}}$  scheme (scheme  $B$  in [10]), it is appropriate to also present the cross sections for process (2.1) in the latter scheme, which was not done in [10]. In this case we have to replace  $C$  by  $B$  in (2.8) and use the transition functions  $\Gamma_{ij}^{DB}$  to change from the DY to the  $\overline{\text{MS}}$  scheme. Since the DY correction term in (2.10) is also known in the  $\overline{\text{MS}}$  scheme up to  $O(\alpha_s^2)$  [4] the appropriate transition functions can be inferred from (2.11) where  $C$  is replaced by  $B$ . Therefore the  $O(\alpha_s)$  corrected cross sections in the  $\overline{\text{MS}}$  scheme are given by

$$\begin{aligned} \left[ s^2 \frac{d^2 \hat{\sigma}_{q\bar{q}}^{(1)}}{dt du} \right]^B &= \left[ s^2 \frac{d^2 \hat{\sigma}_{q\bar{q}}^{(1)}}{dt du} \right]^D \Big|_{\kappa^2=s} \\ &+ \frac{1}{48} \alpha g^2 \frac{\alpha_s(R^2)}{\pi} C_F \left\{ \left[ Q_1(s+t)u + Q_2(M_W^2 - u)t \right]^2 \left[ u^2(s+t)^2 + t^2(M_W^2 - u)^2 + 2sM_W^2(M_W^2 - u)(s+t) \right] \right. \\ &\quad \times \left[ (s+t)^2 + (M_W^2 - u)^2 \right] \left[ \ln \frac{(s_4 - M_W^2)^2}{(s+t)(M_W^2 - u)} + \ln \frac{s}{M^2} \right] \\ &\quad \times u^{-1} t^{-1} (s+t)^{-2} (M_W^2 - u)^{-2} (tM_W^2 + su)^{-2} (s_4 - M_W^2)^{-1} \\ &\quad \left. \times \theta \left[ \frac{s_4 - M_W^2 - \Delta}{s+t} \right] + (t \leftrightarrow u, Q_1 \leftrightarrow Q_2) \right\} \\ &+ \frac{1}{2} \frac{\alpha_s(R^2)}{\pi} C_F \left\{ \delta(s_4 - M_W^2) B_{\text{QED}}(s, t, u, M_W^2) \left[ \left[ 2 \ln \frac{\Delta}{s+t} + \frac{3}{2} \right] \ln \frac{s}{M^2} + 2 \ln^2 \frac{\Delta}{s+t} - 4 + 2\zeta(2) \right] \right. \\ &\quad \left. + (t \leftrightarrow u, Q_1 \leftrightarrow Q_2) \right\}, \end{aligned} \quad (2.23)$$

and

$$\begin{aligned} \left[ s^2 \frac{d^2 \hat{\sigma}_{qg}}{dt du} \right]^B &= \left[ s^2 \frac{d^2 \hat{\sigma}_{qg}}{dt du} \right]^D \Big|_{\kappa^2=s} \\ &+ \frac{1}{48} \alpha g^2 \frac{\alpha_s(R^2)}{\pi} T_f \left\{ \left[ Q_1(M_W^2 - t)u + Q_2(s+u)t \right]^2 \left[ t^2(s+u)^2 + u^2(M_W^2 - t)^2 + 2sM_W^2(M_W^2 - t)(s+u) \right] \right. \\ &\quad \times \left[ (s+u)^2 - 2(M_W^2 - t)(s+u) + 2(M_W^2 - t)^2 \right] \left[ \ln \frac{(s_4 - M_W^2)^2}{(s+u)(M_W^2 - t)} + \ln \frac{s}{M^2} \right] \\ &\quad \left. + \frac{1}{2} (s_4 - M_W^2) [s+u+7(M_W^2 - t)] \right\} u^{-1} t^{-1} (s+u)^{-3} (M_W^2 - t)^{-2} (M_W^2 + st)^{-2} \\ &+ \frac{1}{48} \alpha g^2 \frac{\alpha_s(R^2)}{\pi} T_f \left\{ Q_2^2 \left[ (M_W^2 - s)^2 u^2 + (t+u)^2 s^2 + 2tM_W^2(t+u)(M_W^2 - s) \right] \right. \\ &\quad \times \left[ (t+u)^2 - 2(M_W^2 - s)(t+u) + 2(M_W^2 - s)^2 \right] \ln \left[ \frac{s}{M^2} \right] \\ &\quad \left. \times s^{-1} u^{-1} (t+u)^{-3} (M_W^2 - s)^{-2} \right\}. \end{aligned} \quad (2.24)$$

<sup>3</sup>Equation (7.19) has a typographical error which is corrected here.

<sup>4</sup>Equation (6.33) contains errors. The first square brackets on p. 279 should be moved in front of the coefficient of the logarithm. Also the argument of the logarithm should contain an extra factor of  $(u+t)^2(s-M_W^2)^{-2}$ .

where the expression for  $\sigma_{\bar{q}q}$  can be inferred from (2.24) by the interchanges  $t \leftrightarrow u, Q_1 \leftrightarrow Q_2$ . Regarding the term in (2.24) proportional to  $Q_2^2$  the same comments apply as below (2.22).

In Sec. IV we will examine experimental predictions for the inclusive differential spectra and rates for the reaction  $p + \bar{p} \rightarrow W^+ + \gamma + X$  based on these formulas.

### III. HIGHER-ORDER APPROXIMATIONS

In Ref. [10] we found that the  $O(\alpha_s)$  correction from the  $d\sigma^D$  piece in the  $q\bar{q}$  channel is small relative to the second terms in (2.21) (DIS scheme). We also checked that the total contributions from the  $qg$  and  $g\bar{q}$  channels were small and could be neglected for the CERN  $Spp\bar{p}S$  collider [however we did not check the relative magnitude of the  $d\sigma^D$  terms relative to the second terms in (2.22)]. Therefore, the whole size of the cross section and

shape of the inclusive differential distributions at low energies can be attributed to the second terms in (2.21). The same conclusion holds for the expressions (2.23) and (2.24) which are computed in the  $\overline{\text{MS}}$  scheme. Therefore, we can try to approximate the cross section in both the DIS ( $C$ ) scheme as well as in the  $\overline{\text{MS}}$  ( $B$ ) scheme by dropping all the  $d\sigma^D$  terms on the right-hand sides of Eqs. (2.21)–(2.24). Because the second terms in these same equations originate from the convolution of the transition function  $\Gamma^{DC}$  or  $\Gamma^{DB}$  with the Born cross section (2.4) there is a close similarity between the DY process and the reaction (2.1). Notice that the  $\Gamma^{DC}$  and  $\Gamma^{DB}$  are nothing but the Wilson coefficients of the DY cross section in the DIS and  $\overline{\text{MS}}$  schemes. Since it is extremely difficult to compute the QCD corrections to the reaction  $p + \bar{p} \rightarrow W^+ + \gamma + X$  exactly in  $O(\alpha_s^2)$  and higher we must try to estimate them. With that in mind we propose the first approximation formula

$$s^2 \frac{d^2 \hat{\sigma}_{ij}(s, t, u, R^2, M^2)}{dt du} = \int_0^1 \frac{dx_1}{x_1} \int_0^1 \frac{dx_2}{x_2} \Gamma_{qi}(x_1, s, R^2, M^2) \Gamma_{\bar{q}j}(x_2, s, R^2, M^2) \left[ \hat{s}^2 \frac{d^2 \hat{\sigma}_{q\bar{q}}^{(0)}(\hat{s}, \hat{t}, \hat{u})}{d\hat{t} d\hat{u}} \right], \quad (3.1)$$

where  $d\hat{\sigma}_{q\bar{q}}^{(0)}$  is the Born cross section presented in (2.4). The finite transition functions  $\Gamma_{qi}$  denote the transition from the DY ( $D$ ) scheme to any other scheme, evaluated at the scale  $\kappa = \sqrt{s}$ . Since these are known up to order  $\alpha_s^2$  in both the  $\overline{\text{MS}}$  [4] and in the DIS [5] schemes we are able to compute (3.1) up to order  $\alpha_s^2$ .

We will see in the next section that this first approximation (later called APP1) has problems. Considering also that the  $O(\alpha_s^2)$  contributions to  $\Gamma_{qi}$  are very long it is more practical to make a second approximation (later called APP2) to obtain our final  $O(\alpha_s^2)$  correction to  $d\hat{\sigma}_{q\bar{q}}^{(0)}$ . The latter approximation is based, on the following considerations. For a very long time it is known (see [18–20]) that the DY Wilson coefficient  $\Delta_{ij}$  in (2.10) is dominated by soft-plus-virtual-gluon corrections which originate from the  $q\bar{q}$  process. However as is discussed in [5] this is only true if the c.m. energy is not too large.

As the c.m. energy increases one cannot neglect the hard-gluon radiation in the  $q\bar{q}$  process and the total contributions from the  $qg$  and  $\bar{q}g$  channels anymore. The same effect has been observed for reaction (2.1) in [10]. Notice that the above considerations only hold when the corrections are calculated in the DIS ( $C$ ) scheme. In the  $\overline{\text{MS}}$  ( $B$ ) scheme it is the hard-gluon rather than the soft-gluon contributions which constitute the bulk of the corrections to the  $q\bar{q}$  process. The above findings were based on a comparison in [4,5,10] between the exact cross section and the “soft-plus-virtual-gluon approximation.” In the case of process (2.1) the latter is obtained by taking the soft-gluon limit  $s_4 \rightarrow M_W^2$  in (2.21). Dropping the first term on the right-hand side, i.e.,  $d\sigma^D$  in (2.21), and taking this limit, we get our second and final approximate  $O(\alpha_s)$  correction (in the DIS scheme):

$$\begin{aligned} \left[ s^2 \frac{d^2 \hat{\sigma}_{q\bar{q}}^{(1)}}{dt du} \right]^C &= \frac{\alpha_s(R^2)}{\pi} C_F \left\{ \left[ \ln \frac{(s_4 - M_W^2)^2}{(s+t)(s+u)} + \frac{3}{2} + 2 \ln \frac{s}{M^2} \right] (s_4 - M_W^2)^{-1} \right. \\ &\quad + \delta(s_4 - M_W^2) \left[ \frac{1}{2} \ln^2 \frac{\Delta}{s+t} + \frac{1}{2} \ln^2 \frac{\Delta}{s+u} + \frac{3}{4} \ln \frac{\Delta^2}{(s+t)(s+u)} + 4\zeta(2) + \frac{1}{2} \right. \\ &\quad \left. \left. + \left[ \frac{3}{2} + \ln \frac{\Delta^2}{(s+t)(s+u)} \right] \ln \frac{s}{M^2} \right] \right\} B_{\text{QED}}(s, t, u, M_W^2). \quad (3.2) \end{aligned}$$

Note that we have now dropped completely the contributions from the  $qg$  and  $\bar{q}g$  channels rather than only the  $d\sigma_D$  terms as in our first approximation. (A similar method has been used in [21] to estimate the higher-order corrections to heavy flavor production near threshold.)

We will show in the next section that this is actually a better approximation than taking (3.1), and it can also be extended to higher order as follows.

In order to obtain the  $O(\alpha_s^2)$  corrections to (2.21) and therefore to (3.2) one has first to determine  $\Gamma_{q\bar{q}}^{DC}$  in the

same soft-plus-virtual-gluon approximation, which is easier than calculating the complete function. The latter can be derived from the exact expressions in [5] and its hard and soft-plus-virtual parts are presented in (A4) and (A5), respectively. After the substitution of  $\Gamma_{q\bar{q}}^{DC}$  in (3.1) one obtains the  $O(\alpha_s^2)$  soft-plus-virtual-gluon approximation for  $d\hat{\sigma}_{q\bar{q}}^{(2)}$  in the DIS scheme which is given in (B1) and (B2).

In [10] we checked that the  $O(\alpha_s)$  soft-plus-virtual-gluon approximation in (3.2) gives a fair description of the exact cross section at the c.m. energy  $\sqrt{S}=0.63$  TeV. However at  $\sqrt{S}=1.8$  TeV the approximation gets worse due to the neglect of both the hard-gluon radiation effects and the competing reactions  $qg$  and  $\bar{q}g$ . These studies were done with the mass factorization and renormalization scales set equal to  $\sqrt{s}$ , the parton-parton c.m. energy. The same effect has been observed for the DY reaction in [5] where also the exact  $O(\alpha_s^2)$  contribution has been computed in the DIS scheme. A comparison between the latter and the corresponding  $O(\alpha_s^2)$  soft-plus-virtual-gluon approximation reveals even larger deviations than those already observed at the  $O(\alpha_s)$  level (see Table 4 in [5]), when the scales are set equal to  $M_W$ . Therefore, the corresponding approximation to (3.2) in the DY reaction overestimates the exact  $O(\alpha_s)$  as well as the  $O(\alpha_s^2)$  results at  $\sqrt{S}=0.63$  TeV and  $\sqrt{S}=1.8$  TeV on account of the large negative contributions from the analogous missing terms. However we can remedy this by using the property that the approximate corrections are generally more sensitive to the choice of mass factorization and renormalization scales than the exact ones. Therefore, one can correct for the difference between the exact and approximate expressions by readjusting the scales in such a way that the approximate cross section becomes equal to the exact one. This procedure has been

successfully applied to both  $W$  production and  $Z$  production at  $\sqrt{S}=0.63$  TeV (see Fig. 13 in [5]). By choosing the scales  $M=R=1.8M_W$  and  $M=R=1.8M_Z$ , respectively, in the soft-plus-virtual-gluon approximations, one is able to reproduce the exact cross sections. The above result holds both for the  $O(\alpha_s)$  as well as the  $O(\alpha_s^2)$ -corrected cross sections. This implies that the scale choice does not depend on the order in  $\alpha_s$  in which the cross section is computed. We therefore assume that this also happens for the reaction (2.1).

In the next section we will present numerical results for the total cross sections as well as inclusive photon distributions. Up to order  $\alpha_s$  we use the exact cross sections as represented in Eqs. (2.21)–(2.24) including their dependence on the scales  $M$  and  $R$ . We compare these exact results with those from approximations (3.1) and (3.2) to check that the latter is actually better. Then we give results for the  $O(\alpha_s^2)$  soft-plus-virtual-gluon approximation using the formulas in Appendix B.

#### IV. RESULTS

In this section we will study total cross sections as well as the inclusive differential distributions of the photon. Here we shall limit ourselves to reaction (2.1) where a  $W^+$  is produced. The features of the cross sections for the  $W^-$  are the same as those observed for the  $W^+$  and will therefore not be separately discussed in this paper. The photon inclusive differential distributions can be derived from the expressions for the partonic cross sections in the following way. Denoting the hadronic reaction by

$$p(P_1) + \bar{p}(P_2) \rightarrow W^+(q) + \gamma(k) + X, \quad (4.1)$$

the corresponding hadronic cross section is

$$S^2 \frac{d^2\sigma(S, T, U)}{dT dU} = \int_{x_{1-}}^1 \frac{dx_1}{x_1} \int_{x_{2-}}^1 \frac{dx_2}{x_2} H_{lm}^{W^+}(x_1, x_2, M^2) s^2 \frac{d^2\sigma_{lm}(s, t, u, R^2, M^2)}{dt du}, \quad (4.2)$$

where the lower limits are

$$x_{1-} = \frac{M_W^2 - U}{S + T}, \quad x_{2-} = \frac{M_W^2 - x_1 T}{x_1 S + U}, \quad (4.3)$$

respectively. Here  $d^2\sigma_{lm}$  denote the exact or approximate parton cross sections mentioned in the previous section, where  $l$  corresponds to a parton from the proton in (4.1) and  $m$  to a parton from the antiproton.  $S$ ,  $T$ , and  $U$  denote the square of the hadron c.m. energy and the square of the momentum transfer between the photon and the proton and between the photon and the antiproton, respectively. They are defined by

$$S = (P_1 + P_2)^2, \quad T = (P_1 - k)^2, \quad U = (P_2 - k)^2. \quad (4.4)$$

The quantities  $x_1, x_2$  are the fractions of the momenta of the incoming hadrons which are carried by the partons  $l$  and  $m$ , respectively. The parton kinematic variables now become

$$s = x_1 x_2 S, \quad t = x_1 T, \quad u = x_2 U. \quad (4.5)$$

The integration boundaries in (4.3) are derived from the conditions

$$0 < x_1 < 1, \quad 0 < x_2 < 1, \quad s_4 = x_1 x_2 S + x_1 T + x_2 U \geq M_W^2, \quad (4.6)$$

where  $s_4$  is defined below (2.3). Finally  $H_{lm}^{W^+}(x_1, x_2, M^2)$  are products of factorization-scale-dependent parton densities. For the  $q\bar{q}$  subprocess we have

$$H_{q\bar{q}}^{W^+}(x_1, x_2, M^2) = \{u^p(x_1, M^2)\bar{d}^{\bar{p}}(x_2, M^2) + c^p(x_1, M^2)\bar{s}^{\bar{p}}(x_2, M^2)\} \cos^2\theta_C \\ + \{u^p(x_1, M^2)\bar{s}^{\bar{p}}(x_2, M^2) + c^p(x_1, M^2)\bar{d}^{\bar{p}}(x_2, M^2)\} \sin^2\theta_C, \quad (4.7)$$

and

$$H_{q\bar{q}}^{W^+}(x_1, x_2, M^2) = \{\bar{d}^p(x_1, M^2)u^{\bar{p}}(x_2, M^2) + \bar{s}^p(x_1, M^2)c^{\bar{p}}(x_2, M^2)\} \cos^2\theta_C \\ + \{\bar{s}^p(x_1, M^2)u^{\bar{p}}(x_2, M^2) + \bar{d}^p(x_1, M^2)c^{\bar{p}}(x_2, M^2)\} \sin^2\theta_C, \quad (4.8)$$

where we have only assumed four flavors  $u$ ,  $d$ ,  $s$ , and  $c$ . The Cabibbo angle is chosen to be  $\sin^2\theta_C = 0.05$  while the other angles and/or phases of the Kobayashi-Maskawa matrix are set equal to zero. For  $q(\bar{q})g$  subprocesses the  $H_{lm}^{W^+}$  are given by

$$H_{qg}^{W^+}(x_1, x_2, M^2) = \{u^p(x_1, M^2) + c^p(x_1, M^2)\}g^{\bar{p}}(x_2, M^2), \quad (4.9)$$

$$H_{g\bar{q}}^{W^+}(x_1, x_2, M^2) = g^p(x_1, M^2)\{\bar{d}^{\bar{p}}(x_2, M^2) + \bar{s}^{\bar{p}}(x_2, M^2)\}, \quad (4.10)$$

$$H_{gq}^{W^+}(x_1, x_2, M^2) = \{\bar{d}^p(x_1, M^2) + \bar{s}^p(x_1, M^2)\}g^{\bar{p}}(x_2, M^2), \quad (4.11)$$

and

$$H_{gq}^{W^+}(x_1, x_2, M^2) = g^p(x_1, M^2)\{u^{\bar{p}}(x_2, M^2) + c^{\bar{p}}(x_2, M^2)\}. \quad (4.12)$$

The corresponding cross sections satisfy

$$\left[ S^2 \frac{d^2\sigma(S, T, U)}{dT dU} \right]^B \\ = \int_{x_1-}^1 \frac{dx_1}{x_1} \frac{1}{M_W^2 - x_1 T} \left\{ H_{q\bar{q}}^{W^+} \left[ x_1, \frac{M_W^2 - x_1 T}{x_1 S + U}, M^2 \right] B_{\text{QED}} \left[ \frac{x_1(M_W^2 - x_1 T)}{x_1 S + U}, S, x_1 T, \frac{M_W^2 - x_1 T}{x_1 S + U}, U \right] \right. \\ \left. + H_{q\bar{q}}^{W^+} \left[ x_1, \frac{M_W^2 - x_1 T}{x_1 S + U}, M^2 \right] B_{\text{QED}} \left[ \frac{x_1(M_W^2 - x_1 T)}{x_1 S + U}, S, \frac{M_W^2 - x_1 T}{x_1 S + U}, U, x_1 T \right] \right\}. \quad (4.14)$$

In the case of higher-order corrections one has to distinguish between processes with and without gluons in the final state. If there are gluons in the final state like in the  $q\bar{q}$  subprocess we have to distinguish between soft ( $s_4 < M_W^2 + \Delta$ ) and hard ( $s_4 > M_W^2 + \Delta$ ) gluons, (see (4.6) and the discussion in Sec. 7 of Ref. [10]). Here  $\Delta$  is a parameter which is taken to be zero when soft-plus-virtual-and-hard-gluon contributions are added. If the soft-plus-virtual-gluon piece in the parton cross section is denoted by [see (3.2) and (B2)]

$$\left[ S^2 \frac{d^2\sigma_{q\bar{q}}}{dt du} \right]^{S+V} = \delta(s_4 - M_W^2) \sigma^{S+V}(s, t, u, R^2, M^2, \Delta), \quad (4.15)$$

$$\frac{d^2\sigma_{lm}(s, t, u, R^2, M^2)}{dt du} = \frac{d^2\sigma_{ml}(s, u, t, R^2, M^2)}{dt du}. \quad (4.13)$$

Since the parton cross sections have been computed in both the DIS and the  $\overline{\text{MS}}$  schemes we need the corresponding quark and gluon densities. Here we will use the Morfin-Tung (MT) [16],  $B2$  parametrizations in either the DIS or the  $\overline{\text{MS}}$  schemes (Tables 7 and 8 in [16], respectively). This parametrization provides us with a gluon density  $g^p(x, M^2)$  which rises steeply as  $x \rightarrow 0$  [Lipatov Pomeron where  $xg^p(x, M^2) \approx x^{-1/2}$ ].

Renormalization of the strong-coupling constant has to be performed for the first time when calculating the  $O(\alpha_s^2)$  contribution to the  $q\bar{q}$  process as presented in Appendix B. Here we have chosen the  $\overline{\text{MS}}$  scheme. For the running coupling constant we therefore adopt expression 10 in Ref. [22] where the heavy flavor thresholds have been included. The number of light flavors will be taken equal to 5 even for  $\sqrt{S} = 1.8$  TeV (Tevatron).

Using (2.4), (4.2), (4.13), and the constraint (4.6), the Born contribution to the hadronic cross section takes the form

then the hadronic analogue is given by (4.14) where  $B_{\text{QED}}$  is replaced by  $\sigma^{S+V}$ . The hard-gluon contribution to the hadronic cross section can be obtained from (4.2) by replacing  $x_{2-}$  in (4.3) by

$$x_{2-} = \frac{\Delta + M_W^2 - x_1 T}{x_1 S + U}. \quad (4.16)$$

In reactions (2.7) there are no gluons in the final state so one can simply use expression (4.2) with  $\Delta = 0$ .

The total cross section for (4.1) diverges when the photon energy is soft or when the photon direction becomes collinear with the momenta of the incoming massless partons. To avoid these regions one has to impose cuts on the energy and angle of the photon, which we have

chosen as  $E_\gamma > 10$  GeV, and  $0.1 \text{ rad} < \theta_\gamma < (\pi - 0.1) \text{ rad}$ .  $E_\gamma$  is the energy of the photon in the c.m. system of the proton-antiproton collision and  $\theta_\gamma$  is the angle of the photon in the same system with respect to the proton beam direction.

The Born cross section is dominated by the parton subprocess  $u + \bar{d} \rightarrow W^+ + \gamma$  so that the radiation zero in  $d\sigma/d\cos\theta_\gamma$  (2.5) occurs at  $\cos\theta_\gamma = (Q_1 + Q_2)/(Q_1 - Q_2) = -1/3$ . However, as has been discussed in the literature (see, e.g., Refs. [10–12]), this zero only appears on the partonic level provided one works in the Born approximation. When higher-order QCD corrections are included the soft-plus-virtual part of the  $q\bar{q}$  process leaves the zero intact. However, the zero will be removed by the hard-gluon radiation in the  $q\bar{q}$  subprocess and by the contributions due to the  $qg$  and  $\bar{q}g$  subprocesses. In the case of the hadronic reaction the zero will be already turned into a dip on the Born level due to the convolution with the parton densities. If we include higher-order QCD corrections in the computation of  $d\sigma/d\cos\theta_\gamma$ , then the dip will be further filled in by the hard-gluon bremsstrahlung and contributions from the  $qg$  and  $\bar{q}g$  subprocesses.

Before presenting our results we would like to comment on how the parton cross sections  $d\sigma_{lm}$  and the parton densities depend on the mass factorization scale  $M$  and the renormalization scale  $R$ . Although the anomalous dimensions which determine the scale evolution of the parton densities depend on both the renormalization as well as mass factorization (operator renormalization) choice one does not distinguish between  $R$  and  $M$  in the analysis to extract the  $H_{lm}^{W^+}$  from experimental data. Moreover, as has been pointed out for the DY process in Ref. [4] the cross section is much more sensitive to variations in  $M$  than to changes in  $R$ . This is very easy to understand since the Born cross section is independent of  $\alpha_s(R^2)$ . The same argument applies to the process in (4.1) and therefore we also expect only a small dependence of the cross section on  $R$ , which will be seen in our tables. Because of these observations we shall only consider cross sections where  $R$  is put equal to  $M$  in the parton cross section  $d\sigma_{lm}$ . It is thus convenient to introduce the single dimensionless scale quantity  $r = R/M_W = M/M_W$ .

We begin by presenting in Table I the results for the partial  $O(\alpha_s)$  corrections to the cross sections for the reaction  $p + \bar{p} \rightarrow W^+ + \gamma + X$  at  $\sqrt{S} = 0.63$  TeV (CERN Sp $\bar{p}$ S) in the DIS scheme as a function of  $r$ . The components from the individual  $q\bar{q}$ ,  $qg$ , and  $\bar{q}g$  channels, i.e., from (2.21) and (2.22), are listed, split up into the pieces from the first terms (the  $d\sigma^D$  terms which we call  $\sigma^{(a)}$ ) and the second terms (which we call  $\sigma^{(b)}$ ) together with their totals (which we call  $\sigma^{(1)}$ ). We see that the pieces of the  $qg$  and  $\bar{q}g$  contributions are quite small. Further from the entries in the table we also see that the first approximations (3.1) (i.e., dropping all the  $d\sigma^D$  terms), which we call  $\sigma_{\text{APP1}}^{(1)}$ , underestimates the exact answer for all values of  $r$ . Since  $\sigma_{\text{APP1}}^{(1)}$  increases monotonically as  $r$  increases and does not intersect  $\sigma_{\text{exact}}^{(1)}$  there is no obvious criterion for choosing a particular value of  $r$ . However, the ap-

TABLE I.  $O(\alpha_s)$  corrections to the DIS scheme partial cross sections for  $p + \bar{p} \rightarrow W^+ + \gamma + X$  in  $pb$ , with  $M_W = 80$  GeV/ $c^2$  and  $\sqrt{S} = 0.63$  TeV.

$r$	0.50	0.56	1.0	2.0
$\alpha_S$	0.146	0.143	0.129	0.116
$\sigma_{q\bar{q}}^{(a)}$	0.55	0.53	0.44	0.37
$\sigma_{q\bar{q}}^{(b)}$	2.38	2.43	2.65	2.81
$\sigma_{q\bar{q}}^{(1)}$	2.93	2.96	3.09	3.18
$\sigma_{qg}^{(a)}$	-0.07	-0.07	-0.06	-0.04
$\sigma_{qg}^{(b)}$	0.07	0.05	-0.03	-0.10
$\sigma_{qg}^{(1)}$	0.00	-0.02	-0.09	-0.14
$\sigma_{\bar{q}g}^{(a)}$	-0.17	-0.16	-0.12	-0.09
$\sigma_{\bar{q}g}^{(b)}$	0.06	0.04	-0.01	-0.04
$\sigma_{\bar{q}g}^{(1)}$	-0.11	-0.12	-0.13	-0.13
$\sigma_{qg}^{(1)} + \sigma_{\bar{q}g}^{(1)}$	-0.12	-0.14	-0.21	-0.26
$\sigma_{\text{exact}}^{(1)}$	2.81	2.82	2.88	2.92
$\sigma_{\text{APP1}}^{(1)}$	2.50	2.52	2.61	2.69
$\sigma_{\text{APP2}}^{(1)}$	2.55	2.82	3.94	4.86

proximation (3.2), denoted by  $\sigma_{\text{APP2}}^{(1)}$  is an increasing function of  $r$  which intersects  $\sigma_{\text{exact}}^{(1)}$  at  $r = 0.56$ .

Results for the total hadronic cross section for the reaction  $p + \bar{p} \rightarrow W^+ + \gamma + X$  at  $\sqrt{S} = 0.63$  TeV are shown in Table II for  $r$  taking values between 0.50 and 2.00. The first row contains the Born cross section  $\sigma_{\text{DIS}}^{(0)}$  computed in the DIS scheme with the same parton densities and running coupling constant given above. The second and third rows contain the approximate cross sections, that is the Born cross section plus the approximate  $O(\alpha_s)$  corrections, i.e.,  $\sigma_{\text{DIS}}^{(0)} + \sigma_{\text{DIS,APP1}}^{(1)}$  and  $\sigma_{\text{DIS}}^{(0)} + \sigma_{\text{DIS,APP2}}^{(1)}$ , also computed in the DIS scheme. The fourth row contains the exact  $O(\alpha_s)$  cross section calculated in the DIS scheme, which is given by the Born cross section plus the exact  $O(\alpha_s)$  correction, i.e.,  $\sigma_{\text{DIS}}^{(0)} + \sigma_{\text{DIS,exact}}^{(1)}$ . The fifth row contains the exact  $O(\alpha_s)$  cross section computed in the  $\overline{\text{MS}}$  scheme (using the partonic densities given by Table I in Ref. [16]), which is given by the Born cross section plus the exact  $O(\alpha_s)$  correction in the  $\overline{\text{MS}}$  scheme, i.e.,  $\sigma_{\text{MS}}^{(0)} + \sigma_{\text{MS,exact}}^{(1)}$ . We show in the sixth row of Table II the results for the approximate  $O(\alpha_s^2)$  cross section, which is given by the Born cross section plus the exact  $O(\alpha_s)$  correction, plus the approximate  $O(\alpha_s^2)$  correction, i.e.,  $\sigma_{\text{DIS}}^{(0)} + \sigma_{\text{DIS,exact}}^{(1)} + \sigma_{\text{DIS,APP2}}^{(2)}$ , computed in the DIS scheme.

By comparing the fourth and fifth rows of Table II we see that there is a very small dependence on the scheme at  $O(\alpha_s)$ . The results in the  $\overline{\text{MS}}$  scheme are slightly bigger than those in the DIS scheme, and this difference increases with increasing scale  $r$ . In the range studied, however, the difference is never bigger than 0.5%.

The scale dependences of the other (DIS scheme) cross sections is best displayed graphically so we plot them in Fig. 1. We see that the Born cross section,  $\sigma_{\text{DIS}}^{(0)}$ , decreases by 15% when the scale  $r$  increases from 0.5 to 2.0. From Table I we conclude that the  $O(\alpha_s)$  exact correc-

TABLE II. Total hadronic cross section in pb for reaction  $p + \bar{p} \rightarrow W^+ + \gamma + X$  in the DIS scheme with  $M_W = 80 \text{ GeV}/c^2$  and  $\sqrt{S} = 0.63 \text{ TeV}$ .

Cross section	$r=0.50$	$r=0.56$	$r=1.0$	$r=2.0$
$\sigma_{\text{DIS}}^{(0)}$	7.57	7.47	6.98	6.46
$\sigma_{\text{DIS}}^{(0)} + \sigma_{\text{DIS,APP1}}^{(1)}$	10.1	9.99	9.59	9.15
$\sigma_{\text{DIS}}^{(0)} + \sigma_{\text{DIS,APP2}}^{(1)}$	10.1	10.3	10.9	11.3
$\sigma_{\text{DIS}}^{(0)} + \sigma_{\text{DIS,exact}}^{(1)}$	10.4	10.3	9.86	9.38
$\sigma_{\text{MS}}^{(0)} + \sigma_{\text{MS,exact}}^{(1)}$	10.4	10.3	9.88	9.42
$\sigma_{\text{DIS}}^{(0)} + \sigma_{\text{DIS,exact}}^{(1)} + \sigma_{\text{DIS,APP2}}^{(2)}$	11.2	11.3	11.9	12.5

tion,  $\sigma_{\text{DIS,exact}}^{(1)}$ , increases about 3% when the scale  $r$  increases from 0.5 to 2.0, so the net result is that the  $O(\alpha_s)$  total cross section,  $\sigma_{\text{DIS}}^{(0)} + \sigma_{\text{DIS,exact}}^{(1)}$ , decreases by approximately 10% when  $r$  increases from 0.5 to 2.0 (it decreases 9% in the  $\overline{\text{MS}}$  scheme). Although the sensitivity to the scale is reduced in going from the Born approximation to the first-order exact calculation, the latter still decreases monotonically so it is not clear which scale to choose. Hence our results correspond exactly to those observed for the scale dependencies of the cross sections for the DY process, where it took a complete calculation in  $O(\alpha_s^2)$  before the variation of the cross section with  $r$  became flat. Then one could see for which value of  $r$  the  $O(\alpha_s)$  and  $O(\alpha_s^2)$  soft-plus-virtual predictions (approximation 2) matched the same exact cross section. Now we exploit the findings in the DY reaction and examine the

behavior of our  $O(\alpha_s)$  approximate cross section,  $\sigma_{\text{DIS}}^{(0)} + \sigma_{\text{DIS,APP2}}^{(1)}$ , which increases by 12% when the scale increases from 0.5 to 2.0. It intersects the  $\sigma_{\text{DIS}}^{(0)} + \sigma_{\text{DIS,exact}}^{(1)}$  curve at  $r=0.56$ . At this  $r$  value the prediction for the second approximation through  $O(\alpha_s)$  matches (up to three significant digits) the exact  $O(\alpha_s)$  cross section, both taking the value 10.3 pb. [We also see that at this same value of  $r$  the exact  $O(\alpha_s)$  result in the  $\overline{\text{MS}}$  scheme matches the one in the DIS scheme.] Therefore we should use this value in our  $O(\alpha_s^2)$  results given in (B1) and (B2) ( $\sigma_{\text{APP2}}^{(2)}$ ). The final total cross section through  $O(\alpha_s^2)$  can be read from Table II to be 11.3 pb. The  $O(\alpha_s^2)$  correction adds 10% to the exact  $O(\alpha_s)$  total cross section, whereas the  $O(\alpha_s)$  correction adds 38% to the Born approximation, thus making the perturbation series reliable at this value of the scale  $r$ . Based on the findings obtained in the DY process at  $O(\alpha_s^2)$ , we expect that the exact value of the total cross section of the radiative reaction through  $O(\alpha_s^2)$  not to deviate very much from 11.3 pb in the range of  $r$  studied here. Therefore we note that the  $r$  dependence of the  $O(\alpha_s^2)$  approximate total cross section,  $\sigma_{\text{DIS}}^{(0)} + \sigma_{\text{DIS,exact}}^{(1)} + \sigma_{\text{DIS,APP2}}^{(2)}$  included in Table II has no real meaning, it is just given for completeness.

We now examine the inclusive differential distributions to check whether the same constant value  $r=0.56$  works there too. In particular we are interested in the ratios of the APP2 to the exact inclusive distributions (we no longer consider the APP1). If they are not uniformly proportional to each other we might expect to need different  $r_X$  scales, one for each distribution, labeled by  $X = \cos\theta_\gamma$ ,  $X = E_\gamma$ , etc. We therefore define the ratios of the differential cross sections

$$R_X = \frac{d\sigma^{(0)}/dX + d\sigma_{\text{APP2}}^{(1)}/dX}{d\sigma^{(0)}/dX + d\sigma_{\text{exact}}^{(1)}/dX}, \quad (4.17)$$

and plot them versus  $X$  for different values of the scale  $r$ . Figure 2 shows the ratio  $R_{\cos\theta}$  computed for the same four values of  $r$  appearing in Table II. The numerical error on the curves is around 2%. When the ratio is close to 1.0 then we have a good result for the approximate distribution, but if it deviates too much from 1.0 we cannot trust it any more. From Fig. 2 we conclude that at  $r=0.56$  the  $O(\alpha_s)$  approximation for the distribution in  $\cos\theta_\gamma$  is in excellent agreement with the  $O(\alpha_s)$  exact distribution, thus demonstrating that our  $O(\alpha_s^2)$  prediction is also reliable for the angular distribution as well as for the cross section. This is not true at larger values of the

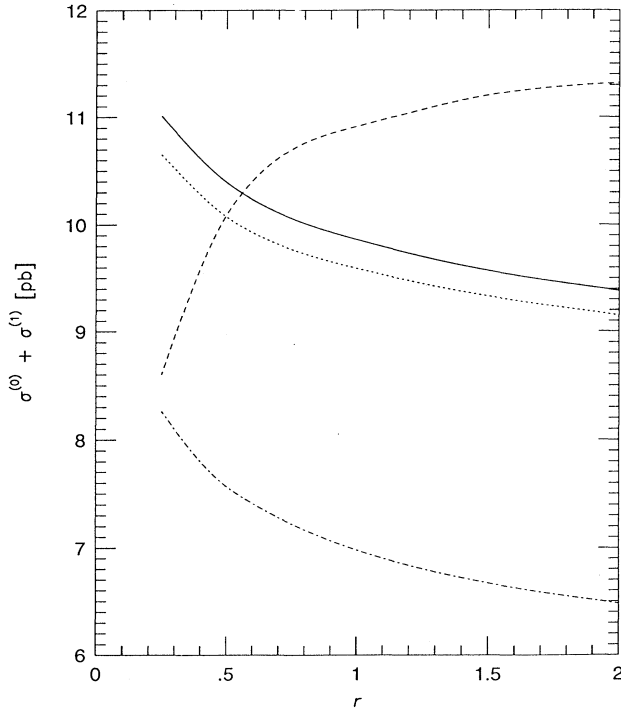


FIG. 1. Total  $O(\alpha_s)$  cross sections computed in the DIS scheme as a function of the scale  $r = M/M_W$  at  $\sqrt{S} = 0.63 \text{ TeV}$ .  $\sigma_{\text{DIS}}^{(0)} + \sigma_{\text{DIS,APP1}}^{(1)}$  is plotted with a solid line,  $\sigma_{\text{DIS}}^{(0)} + \sigma_{\text{DIS,APP2}}^{(1)}$  with a dashed line,  $\sigma_{\text{DIS}}^{(0)} + \sigma_{\text{DIS,APP}}^{(1)}$  with a dotted line, and  $\sigma_{\text{DIS}}^{(0)}$  with a dot-dashed line.

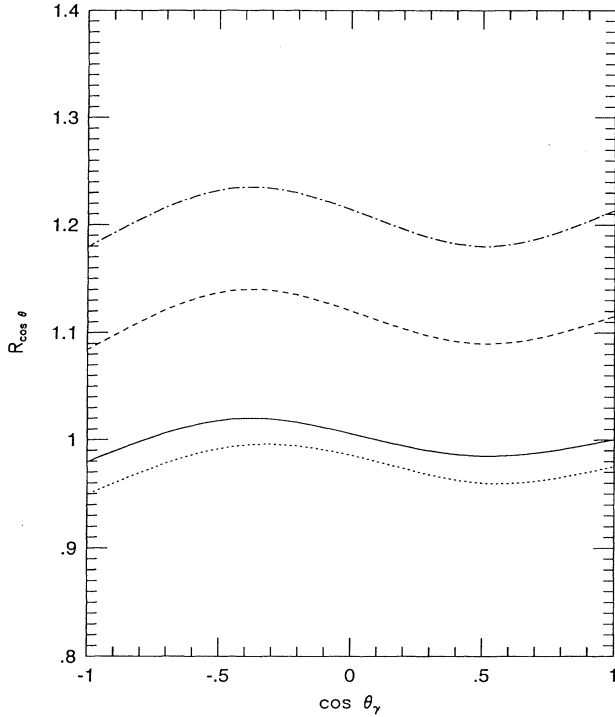


FIG. 2. The ratios  $R_{\cos\theta}$  at the scales  $r=0.50$  (dotted line),  $r=0.56$  (solid line),  $r=1.0$  (dashed line), and  $r=2.0$  (dash-dotted line). The c.m. energy is  $\sqrt{S}=0.63$  TeV.

scale  $r$ : we can see that at  $r$  near 2.0 the deviation introduced at the  $O(\alpha_s)$  level reaches 25%, so we cannot trust the  $O(\alpha_s^2)$  predictions for this distribution at large values of  $r$ .

Figure 3 shows the actual differential cross section in the angular distribution of the photon,  $d\sigma/d\cos\theta_\gamma$ . It shows the Born differential cross section, i.e.,  $d\sigma^{(0)}/d\cos\theta_\gamma$ , the  $O(\alpha_s)$  exact differential cross section

$$\frac{d\sigma^{(0)}}{d\cos\theta_\gamma} + \frac{d\sigma_{\text{exact}}^{(1)}}{d\cos\theta_\gamma},$$

and our best estimate for the  $O(\alpha_s^2)$  approximate differential cross section

$$\frac{d\sigma^{(0)}}{d\cos\theta_\gamma} + \frac{d\sigma_{\text{exact}}^{(1)}}{d\cos\theta_\gamma} + \frac{d\sigma_{\text{APP2}}^{(2)}}{d\cos\theta_\gamma}.$$

They have been computed in the DIS scheme using the scale  $r=0.56$  which, as we already discussed, is the best choice for computing the  $O(\alpha_s^2)$ -corrected total cross section at  $\sqrt{S}=0.63$  TeV. Note that this plot is drawn with a semilogarithmic scale. The position of the minimum is at  $\cos\theta_\gamma = -1/3$ .

The corresponding results for the inclusive distributions in the photon rapidity,  $\eta_\gamma = \frac{1}{2} \ln[(1 + \cos\theta_\gamma)/(1 - \cos\theta_\gamma)]$  now follow.  $R_\eta$  is plotted in Fig. 4 and we see excellent agreement for  $r=0.56$ . Figure 5 shows the actual distributions.

Next we turn to the inclusive photon distribution in the energy  $E_\gamma$ , which was defined after (4.16). Figures 6

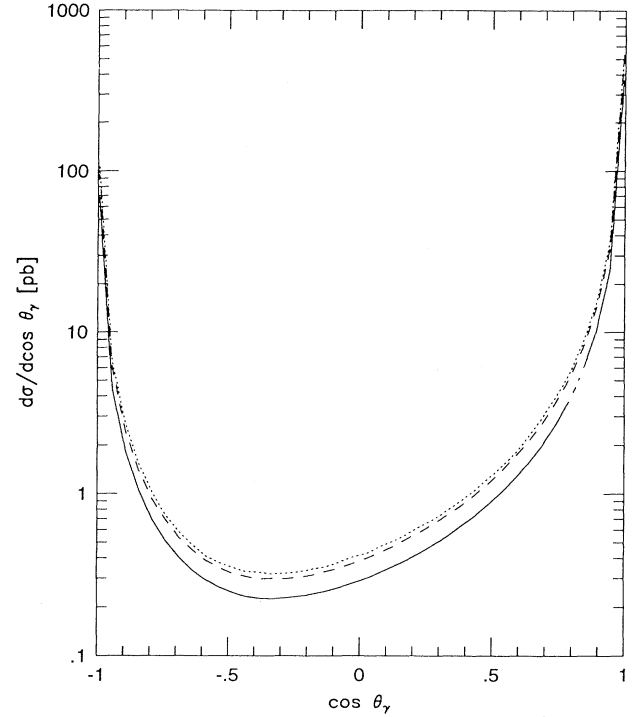


FIG. 3. Photon inclusive differential distributions  $d\sigma/d\cos\theta_\gamma$  in the DIS scheme with  $r=0.56$  at  $\sqrt{S}=0.63$  TeV. The solid curve shows the Born distribution, the dashed curve shows the exact distribution in  $O(\alpha_s)$ , and the dotted curve shows our prediction through  $O(\alpha_s^2)$ .

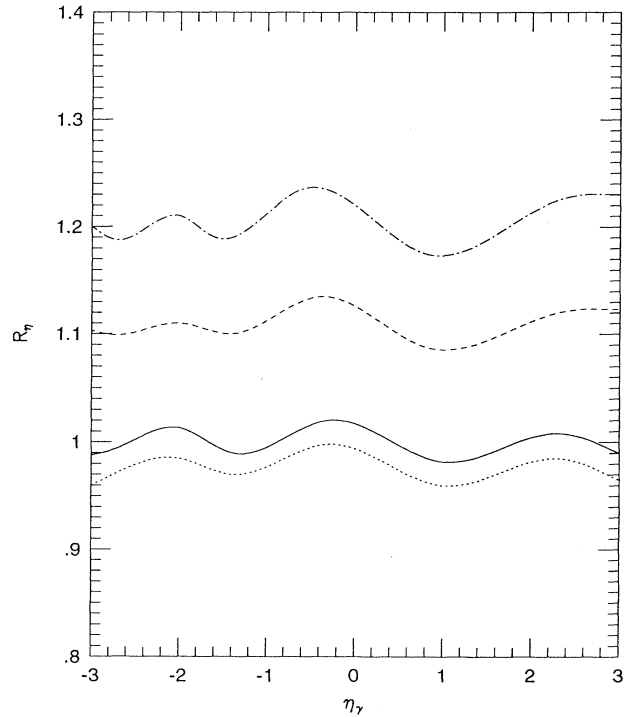


FIG. 4. The ratios  $R_\eta$  at  $\sqrt{S}=0.63$  TeV. The notation is the same as in Fig. 2.

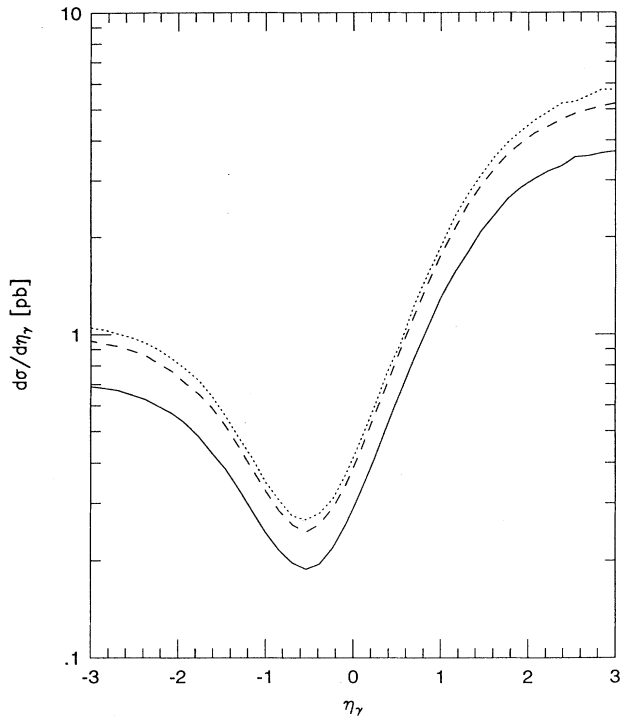


FIG. 5. Photon inclusive differential distributions  $d\sigma/d\eta_\gamma$  in the DIS scheme with  $r=0.56$  at  $\sqrt{S}=0.63$  TeV. The notation is the same as in Fig. 3.

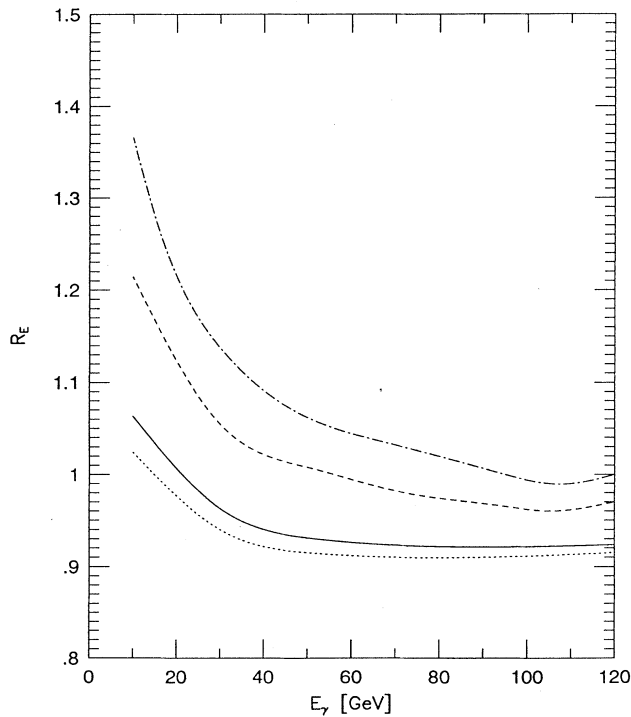


FIG. 6. The ratios  $R_E$  at  $\sqrt{S}=0.63$  TeV. The notation is the same as in Fig. 2.

and 7 show the ratio  $R_E$  and the actual distributions, respectively. Remember that we have imposed a cut at  $E_\gamma=10$  GeV. Because of the rapid fall off in the  $E_\gamma$  distribution we only plotted it out to 120 GeV, while the actual maximal energy is around 310 GeV.

Finally we show the corresponding plots for the inclusive distribution in the transverse momentum of the photon  $p_{t\gamma}=E_\gamma \sin\theta_\gamma$ .  $R_{p_t}$  and  $d\sigma/p_{t\gamma}$  are shown in Figs. 8 and 9, respectively, again only up to 120 GeV.

The last four figures referred to above all demonstrate that the  $O(\alpha_s)$ -corrected APP2 only behaves moderately well for the distributions in  $E_\gamma$  and  $p_{t\gamma}$  at the scale  $r=0.56$ , resulting in deviations of about 8% in the regions where the differential cross sections are large, i.e., for low  $E_\gamma$  and  $p_{t\gamma}$ . This can be understood by noting that the low  $E_\gamma$  and  $p_{t\gamma}$  photons are correlated mainly with the regions of phase space where the hard-gluon radiation and the contributions from the  $qg$ ,  $\bar{q}g$  subprocesses cannot be neglected. Therefore we cannot expect the APP2 to work so well in these regions. On the other hand, high-energy and high-transverse-momentum photons are produced in regions of phase space where the additional emitted gluon becomes soft, and so we expect that APP2 behaves better in these regions. What we actually see in Figs. 6 and 8 is that the  $R_X$  ratios become flat at large values of  $E_\gamma$  and  $p_{t\gamma}$  for all values of the scale  $r$ , but they do not necessarily approach the value 1.0, mainly due to the missing contributions from the  $q(\bar{q})g$  channels, which are dropped in this approximation. If we wanted to make better predictions in the large  $E_\gamma$  and

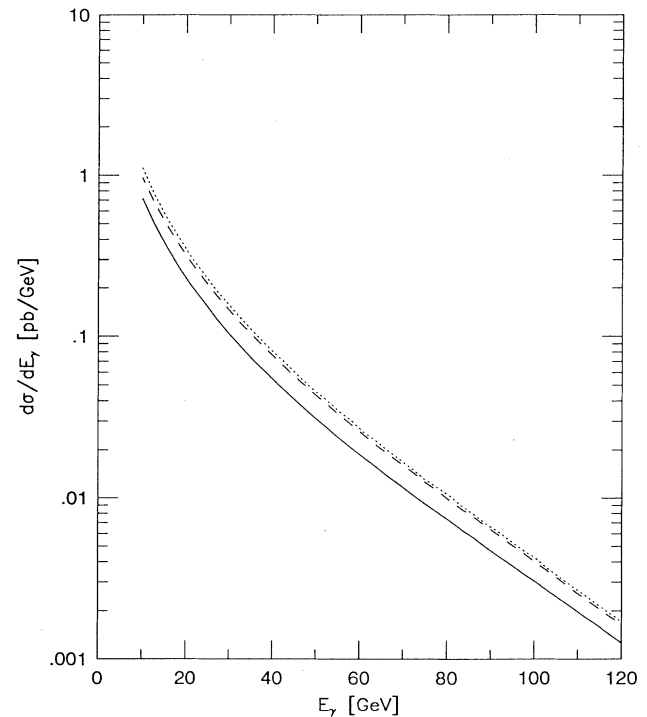


FIG. 7. Photon inclusive differential distributions  $d\sigma/dE_\gamma$  in the DIS scheme with  $r=0.56$  at  $\sqrt{S}=0.63$  TeV. The notation is the same as in Fig. 3.

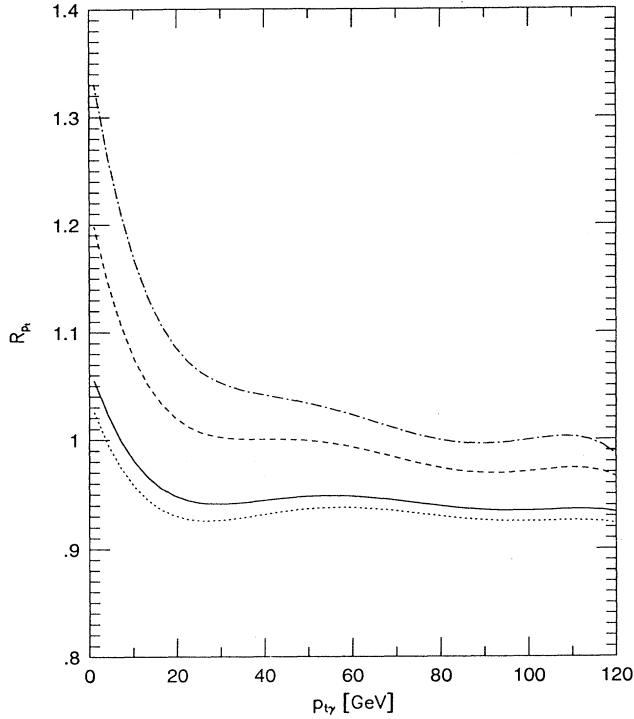


FIG. 8. The ratios  $R_{pt}$  at  $\sqrt{S} = 0.63$  TeV. The notation is the same as in Fig. 2.

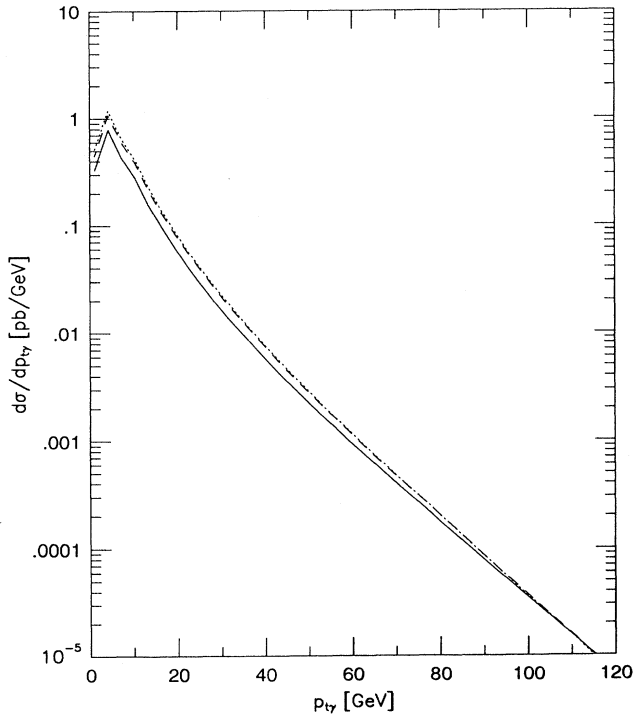


FIG. 9. Photon inclusive differential distributions  $d\sigma/dp_{T\gamma}$  in the DIS scheme with  $r = 0.56$  at  $\sqrt{S} = 0.63$  TeV. The notation is the same as in Fig. 3.

large  $p_{T\gamma}$  regions using our approximation, we could increase the cut in  $E_\gamma$  increasing at the same time the value of the scale  $r$ . For example, by cutting  $E_\gamma$  above 40 GeV we would obtain an excellent  $R_E$  ratio choosing  $r \approx 1.0$ . The same would hold for  $R_{pt}$ . The cost of doing this is that we dramatically reduce the size of the cross section.

From the previous plots we conclude that the shapes of the Born, exact  $O(\alpha_s)$ , and approximate  $O(\alpha_s^2)$  differential cross sections are reasonably similar at  $\sqrt{S} = 0.63$  GeV. Hence the corresponding  $K$  factors for the distributions are flat. The only exception is the  $p_t$  distribution, which as can be seen from Fig. 9, has rapidly decreasing  $K$  factors as the transverse momentum increases.

We conclude this discussion by noting that we have deliberately avoided making the scales in the last four plots functions of  $E_\gamma$  and/or  $p_{T\gamma}$  since this would not allow us to make any connection with the choice of the constant scale in the cross section.

We now consider the higher-energy results for the Fermilab Tevatron at  $\sqrt{S} = 1.8$  TeV. Tables III and IV give the corresponding partial and total cross sections. Now we notice a dramatic increase in the size of the  $qg$  and  $\bar{q}g$  channels. Here APP1 (3.1) yields larger results than the exact answer. Approximation (3.2) shows a monotonic increase as the scale increases. The neglect of the hard radiation contributions in the  $q\bar{q}$  channels and the negative contributions from the  $qg$  and  $\bar{q}g$  channels causes this change in the  $r$  dependence. Since the c.m. energy is multiplied by a factor of 3, the values for the total cross sections in Table IV have increased by roughly the same amount when compared to those in Table II. By comparing the fourth and fifth rows of Table IV we see the same qualitative dependence on the scheme at  $O(\alpha_s)$  as we observed at  $\sqrt{S} = 0.63$  TeV in Table II. At 1.8 TeV, however, the difference between the results in the  $\overline{\text{MS}}$  and the

TABLE III.  $O(\alpha_s)$  corrections to the DIS scheme partial cross sections for  $p + \bar{p} \rightarrow W^+ + \gamma + X$  in  $pb$ , with  $M_W = 80$  GeV/ $c^2$  and  $\sqrt{S} = 1.8$  TeV.

$r$	0.50	0.52	1.0	2.0
$\alpha_S$	0.146	0.145	0.129	0.116
$\sigma_{q\bar{q}}^{(a)}$	1.82	1.81	1.59	1.40
$\sigma_{q\bar{q}}^{(b)}$	8.21	8.24	8.67	9.13
$\sigma_{q\bar{q}}^{(1)}$	10.03	10.04	10.26	10.53
$\sigma_{qg}^{(a)}$	-0.64	-0.64	-0.55	-0.48
$\sigma_{qg}^{(b)}$	1.29	1.21	-0.02	-0.97
$\sigma_{qg}^{(1)}$	0.65	0.57	-0.57	-1.45
$\sigma_{\bar{q}g}^{(a)}$	-3.66	-3.62	-3.03	-2.53
$\sigma_{\bar{q}g}^{(b)}$	1.62	1.53	0.29	-0.65
$\sigma_{\bar{q}g}^{(1)}$	-2.04	-2.09	-2.74	-3.18
$\sigma_{qg}^{(1)} + \sigma_{\bar{q}g}^{(1)}$	-1.39	-1.52	-3.31	-4.63
$\sigma_{\text{exact}}^{(1)}$	8.64	8.52	6.95	5.90
$\sigma_{\text{APP1}}^{(1)}$	11.12	10.97	8.94	7.51
$\sigma_{\text{APP2}}^{(1)}$	8.22	8.55	13.40	17.47

TABLE IV. Total hadronic cross section in  $pb$  for reaction  $p + \bar{p} \rightarrow W^+ + \gamma + X$  in the DIS scheme with  $M_W = 80 \text{ GeV}/c^2$  and  $\sqrt{S} = 1.8 \text{ TeV}$ .

Cross section	$r=0.50$	$r=0.52$	$r=1.0$	$r=2.0$
$\sigma_{\text{DIS}}^{(0)}$	23.7	23.7	23.7	23.6
$\sigma_{\text{DIS}}^{(0)} + \sigma_{\text{APP1}}^{(1)}$	34.5	34.3	33.5	31.2
$\sigma_{\text{DIS}}^{(0)} + \sigma_{\text{APP2}}^{(1)}$	31.9	32.3	37.1	41.0
$\sigma_{\text{DIS}}^{(0)} + \sigma_{\text{DIS,exact}}^{(1)}$	32.4	32.2	30.7	29.5
$\sigma_{\text{MS}}^{(0)} + \sigma_{\text{MS,exact}}^{(1)}$	32.6	32.5	31.2	30.3
$\sigma_{\text{DIS}}^{(0)} + \sigma_{\text{DIS,exact}}^{(1)} + \sigma_{\text{DIS,APP2}}^{(2)}$	35.1	35.2	37.7	40.9

DIS scheme is 3% at a scale  $r=2.0$ , which is still small but larger than the value of 0.5% we found at 0.63 TeV.

Figure 10 shows the plots obtained for the first four rows of Table IV, as functions of the scale  $r$  at 1.8 TeV. We now see clearly that the Born cross section,  $\sigma_{\text{DIS}}^{(0)}$ , shows negligible variation over the whole range of  $r$ . The  $O(\alpha_s)$  exact correction,  $\sigma_{\text{DIS,exact}}^{(1)}$  decreases 30% when the scale  $r$  increases from 0.5 to 2.0, so the net result is that the  $O(\alpha_s)$  total cross section,  $\sigma_{\text{DIS}}^{(0)} + \sigma_{\text{DIS,exact}}^{(1)}$ , decreases 9% through the same range (it decreases 7% in the  $\overline{\text{MS}}$  scheme), which is roughly the same as we got at 0.63 TeV. The behavior of the  $O(\alpha_s)$  approximate cross section  $\sigma_{\text{DIS}}^{(0)} + \sigma_{\text{DIS,APP1}}^{(1)}$  has the same dependence on the scale, i.e., it monotonically decreases with  $r$ , and does not intersect the  $O(\alpha_s)$  exact cross section. The behavior of the  $O(\alpha_s)$  approximate cross section,  $\sigma_{\text{DIS}}^{(0)} + \sigma_{\text{DIS,APP2}}^{(1)}$  is the opposite, as we already observed at 0.63 TeV, and comes out to be much steeper than at 0.63 TeV: it increases almost 30% when the scale is increased from 0.5 to 2.0. Note that the decrease in the exact result and the

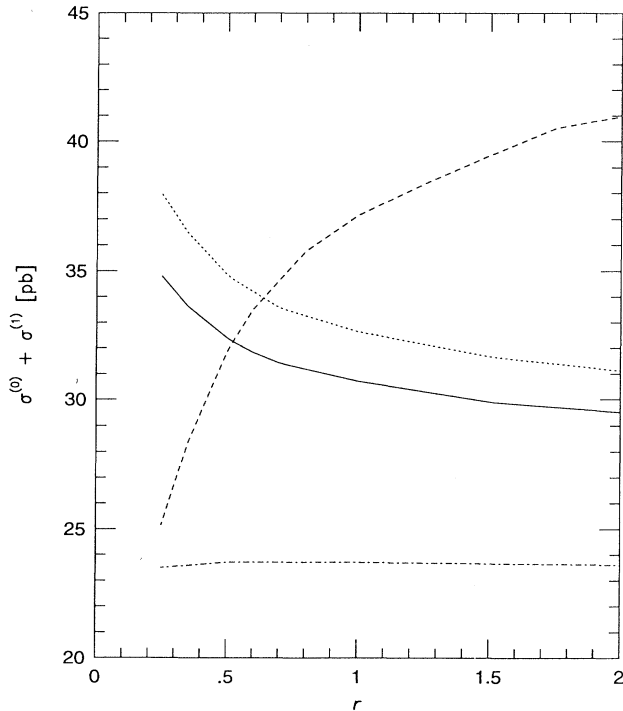


FIG. 10. Same as Fig. 1 for  $\sqrt{S} = 1.8 \text{ TeV}$ .

growth in the approximate result as  $r$  increases is similar to the corresponding DY results in this energy domain.

The best value of the scale  $r$  at 1.8 TeV, obtained in the same way as at the lower energy of 0.63 TeV, is slightly smaller in this case. Up to two significant digits, Table IV and Fig. 10 show that  $r=0.52$ . For this value the prediction of the  $O(\alpha_s)$  approximation gives 32.3 pb, to be compared with the exact total cross section  $O(\alpha_s)$  result of 32.2 pb. At this value the exact  $O(\alpha_s)$  result in the  $\overline{\text{MS}}$  scheme gives 32.5 pb versus 32.2 pb in the DIS scheme, so we can still neglect any difference between the two schemes. From Table IV our best prediction for the total hadronic cross section through  $O(\alpha_s^2)$  is therefore 35.2 pb. In other words the  $O(\alpha_s^2)$  correction adds around 9% to the  $O(\alpha_s)$  exact result whereas the  $O(\alpha_s)$  correction adds 36% to the Born total cross section, so perturbation theory seems to converge well.

We now turn to the distributions at the c.m. energy of 1.8 TeV and compare the results from (3.2) versus the exact ones, using the same inputs as above. The ratio  $R_{\cos\theta}$  which was defined above, is plotted for the c.m. energy of 1.8 TeV in Fig. 11. The fluctuations in the latter plot demonstrate that our  $O(\alpha_s)$  approximation at  $r=0.52$  is not so good at this c.m. energy. However choosing larger values for  $r$  is clearly incorrect. Figure 12 shows the plot of the inclusive differential cross section for the photon variable  $\cos\theta_\gamma$ . The notation is the same as used in Fig. 3 for 0.63 GeV. The ratio  $R_\eta$  and the actual inclusive differential distribution for  $\eta$  are shown in Figs. 13 and 14, respectively.

From these plots we conclude that at the c.m. energy of 1.8 TeV our  $O(\alpha_s)$  approximation in (3.2) with  $r=0.52$  is not so good in predicting these distributions when the photon energy and angle cuts are set equal to 10 GeV and 0.1 rad, respectively. The ratios  $R_{\cos\theta}$  and  $R_\eta$  now show increases of about 10% above unity near  $\cos\theta = -1$  and  $\eta = -3$ , respectively. The deviations are smaller at the opposite ends of the ranges, however (see Figs. 11 and 13 and compare them with Figs. 2 and 4). In contrast with the situation at 0.63 TeV, we observe a big asymmetry in  $R_{\cos\theta}$  and  $R_\eta$  at 1.8 TeV for all values of the scale  $r$ . These ratios are good at the upper ends of the distributions, i.e., in the regions  $\cos\theta_\gamma \approx 1.0$  and  $\eta_\gamma \approx 3.0$ , but they are poor at the other ends of the distributions, i.e., in the regions  $\cos\theta_\gamma \approx -1.0$  and  $\eta_\gamma \approx -3.0$ . This can be understood by noting from Table III that the  $qg$  and  $\bar{q}g$  channels become relatively more important than at 0.63 TeV. At 1.8 TeV these channels are dominated by the reaction  $g + \bar{d} \rightarrow W^+ + \bar{u} + \gamma$  and thus the total con-

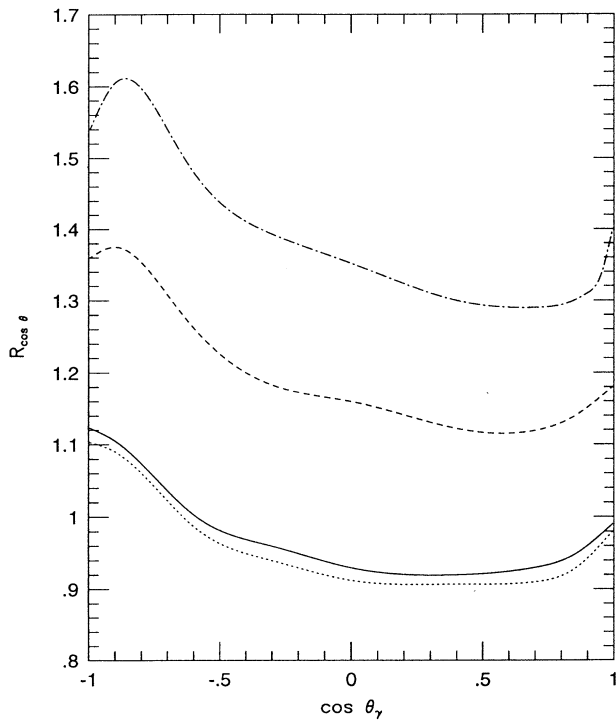


FIG. 11. Same as Fig. 2 for  $\sqrt{S} = 1.8$  TeV and  $r = 0.50, 0.52, 1.0$ , and  $2.0$ .

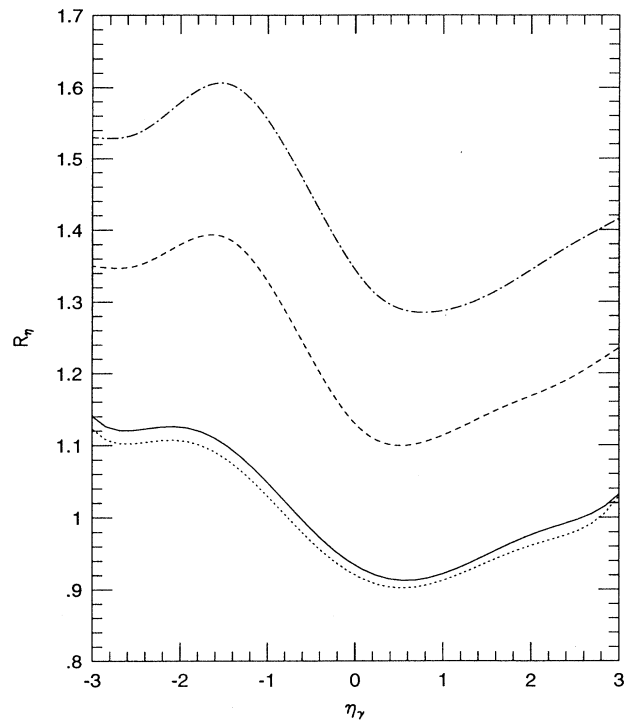


FIG. 13. Same as Fig. 4 for  $\sqrt{S} = 1.8$  TeV and  $r = 0.50, 0.52, 1.0$ , and  $2.0$ .

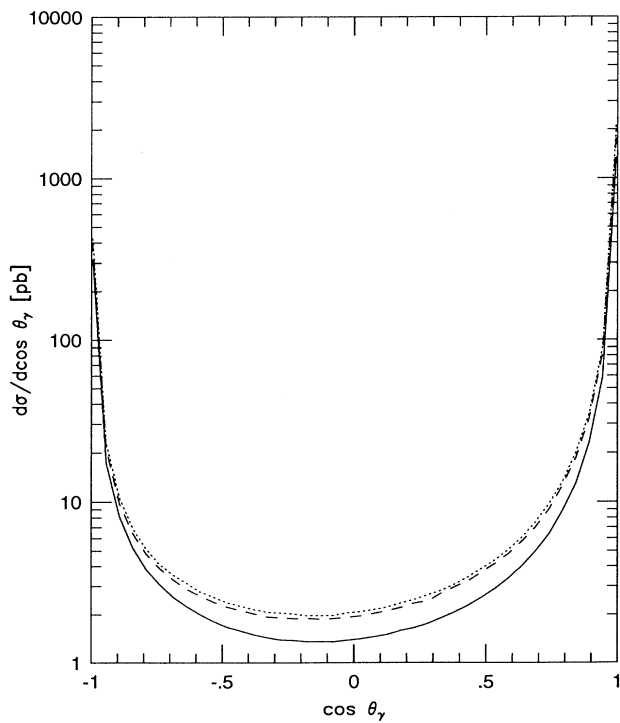


FIG. 12. Same as in Fig. 3 for  $\sqrt{S} = 1.8$  TeV and  $r = 0.52$ .

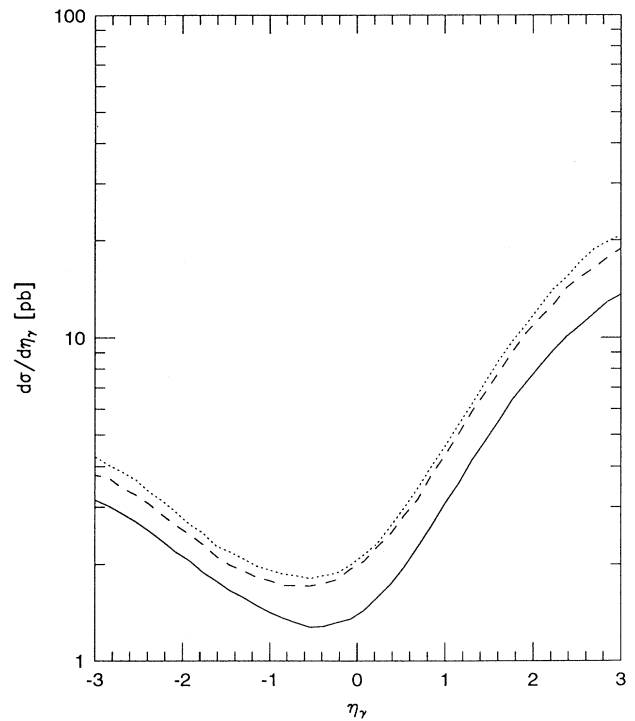


FIG. 14. Same as Fig. 5 for  $\sqrt{S} = 1.8$  TeV and  $r = 0.52$ .

tribution of these channels to the  $\cos\theta_\gamma$  and  $\eta_\gamma$  distributions is asymmetric. This effect can be appreciated in Fig. 15, where we have introduced the ratio  $R_{q(\bar{q})g}$ , which represents the quotient of the contribution of the  $q(\bar{q})g$  channels to the hadronic differential cross section divided by the total differential cross section at  $O(\alpha_s)$ . We see a large negative contribution near  $\cos\theta_\gamma = -1$  and a negligible contribution near  $\cos\theta_\gamma = 1$ . The plots suggest that increasing the cut in the photon angle and appropriately increasing  $r$  would considerably improve the performance of the approximation.

The plots for  $E_\gamma$  and  $R_E$ , as defined above, are shown in Figs. 16 and 17, respectively. We have cut the plot in  $E_\gamma$  at 120 GeV, while the actual maximal  $E_\gamma$  occurs at about 900 GeV. Finally we present the ratio  $R_{p_t}$  and the inclusive distribution in  $p_{t\gamma}$  in Figs. 18 and 19, respectively. The  $R_E$  and  $R_{p_t}$  ratios in Figs. 16 and 18 show bigger deviations from 1.0 than at 0.63 TeV (compare with Figs. 6 and 8, respectively) but the qualitative behavior of these ratios remains the same. Again the plots suggest that we could improve the approximation for these two distributions by cutting at a higher value of the energy  $E_\gamma$  (around 50 GeV in this case) and increasing the scale  $r$ . Like at  $\sqrt{S} = 0.63$  TeV an increase in the angle and energy cuts would considerably reduce the total cross sections.

We have also included the approximate  $O(\alpha_s^2)$  terms in our predictions for the  $E_\gamma$  and  $p_{t\gamma}$  distributions in Figs.

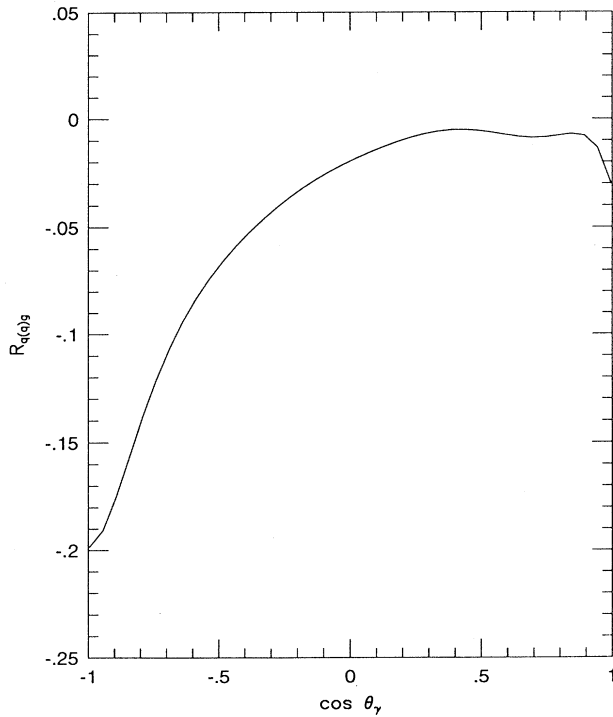


FIG. 15. The ratio  $R_{q(\bar{q})g}$  of the contributions of the  $qg$  and  $\bar{q}g$  channels divided by the total photon inclusive differential distribution computed at  $O(\alpha_s)$  in the DIS scheme for  $\sqrt{S} = 1.8$  TeV and  $r = 0.52$ .

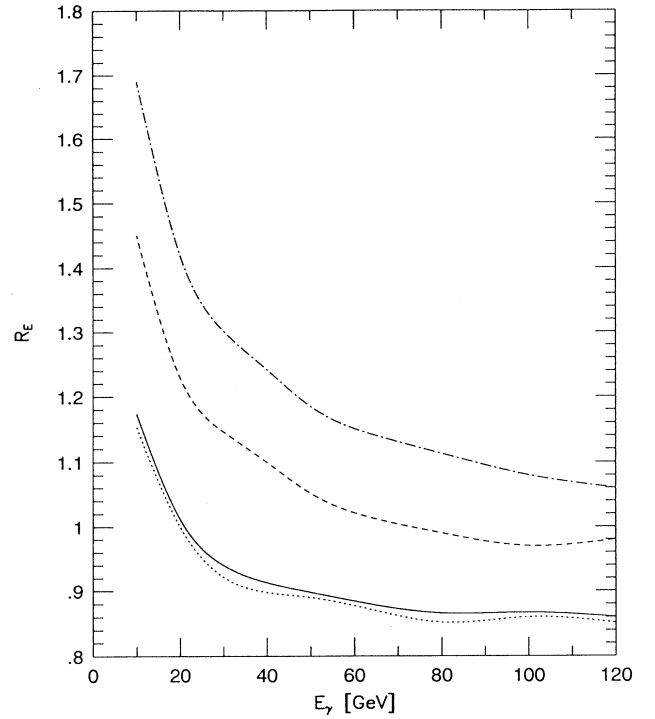


FIG. 16. Same as Fig. 6 for  $\sqrt{S} = 1.8$  TeV and  $r = 0.50, 0.52, 1.0$ , and  $2.0$ .

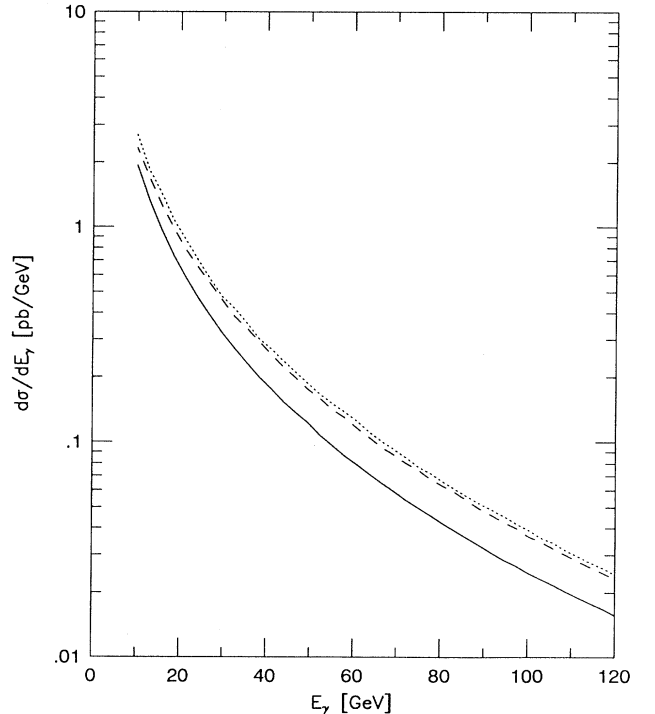


FIG. 17. Same as Fig. 7 for  $\sqrt{S} = 1.8$  TeV and  $r = 0.52$ .

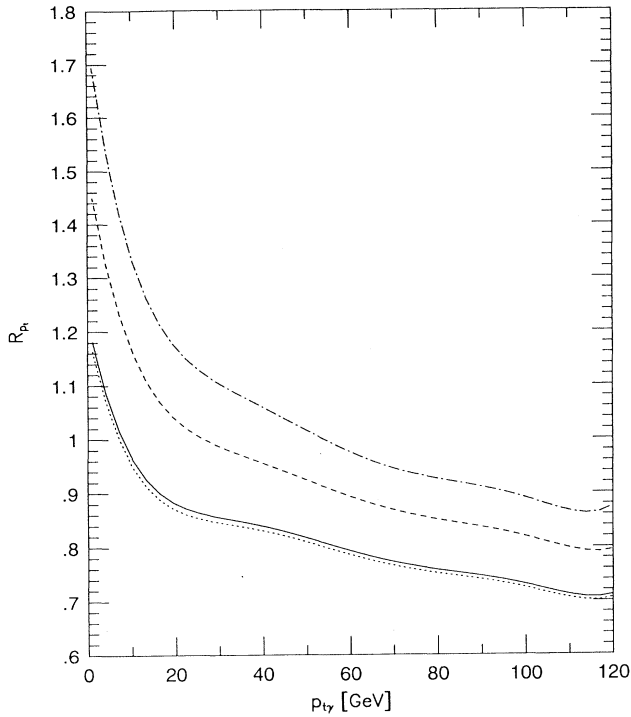


FIG. 18. Same as Fig. 8 for  $\sqrt{S} = 1.8$  TeV and  $r = 0.50, 0.52, 1.0,$  and  $2.0$ .

17 and 19. However as we explained above, since the  $R_X$  ratios are not so good at 1.8 TeV thus we cannot expect such good results at  $O(\alpha_s^2)$  as found for 0.63 TeV.

From the above plots we conclude that the shapes of the Born, exact  $O(\alpha_s)$ , and approximate  $O(\alpha_s^2)$  inclusive differential distributions are not identical at  $\sqrt{S} = 1.8$  TeV. A close examination shows that the corresponding  $K$  factors for the exact  $O(\alpha_s)$  distributions tend to increase as  $\cos\theta_\gamma, \eta_\gamma, E_\gamma,$  and  $p_{T\gamma}$  increase while those for the  $O(\alpha_s^2)$  APP2 are reasonably flat.

To briefly summarize our investigations we have computed the  $O(\alpha_s^2)$  contribution to the reaction  $p + \bar{p} \rightarrow W^+ + \gamma + X$  in the soft-plus-virtual-gluon approximation (called APP2 in this paper) using a value for the mass factorization and renormalization scale  $r$  determined from the comparison between the exact cross section and that predicted by the  $O(\alpha_s)$  approximated one.

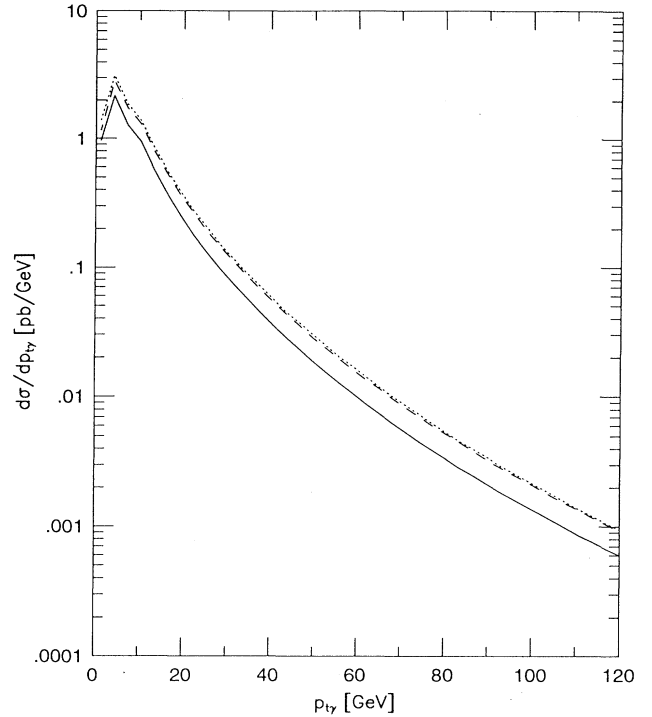


FIG. 19. Same as Fig. 9 for  $\sqrt{S} = 1.8$  TeV and  $r = 0.52$ .

From our plots of the inclusive differential distributions we conclude that the shapes of the Born, exact  $O(\alpha_s)$ , and approximate  $O(\alpha_s^2)$  distributions are not identical at the two energies studied. Therefore there is an error involved if one tries to include these higher-order contributions by multiplying the Born distribution by a constant factor, but this is probably a reasonable thing to do until much more data is available.

#### ACKNOWLEDGMENTS

We would like to thank Jim Ohnemus for a comparison of his results for the  $O(\alpha_s)$  QCD corrections [23] and our results previously reported in [10]. The work in this paper was supported in part under Contract No. NSF 92-11367 and the Texas National Research Laboratory Commission.

#### APPENDIX A

Here we present the functions needed for the transition from the DY scheme to the DIS scheme. Dropping the superscript DC one finds, in lowest order,

$$\Gamma_{qq}^{(0)}(x) = \delta(1-x). \quad (\text{A1})$$

In order  $\alpha_s$  we obtain, from (2.9) and (2.13), (2.14),

$$\Gamma_{qq}^{(1)}(x, \kappa^2, R^2, M^2) = \frac{\alpha_s(R^2)}{\pi} C_F \left[ \left\{ \frac{1+x^2}{1-x} \left[ \frac{1}{2} \ln(1-x) + \frac{3}{8} + \frac{1}{2} \ln \frac{\kappa^2}{M^2} \right] - \frac{9}{8} - \frac{5}{8} x \right\} \theta(1-x-\delta) \right. \\ \left. + \delta(1-x) \left\{ \left[ \ln \delta + \frac{3}{4} \right] \ln \frac{\kappa^2}{M^2} + \frac{1}{2} \ln^2 \delta + \frac{3}{4} \ln \delta + \frac{1}{4} + 2\xi(2) \right\} \right], \quad (\text{A2})$$

and from (2.9) and (2.15), (2.16) one gets

$$\Gamma_{gg}(x, \kappa^2, R^2, M^2) = \frac{\alpha_s(R^2)}{\pi} T_f \left[ \{x^2 + (1-x)^2\} \left[ \frac{1}{2} \ln(1-x) + \frac{1}{2} \ln \frac{\kappa^2}{M^2} + \frac{1}{2} \right] + \frac{1}{4} (1-x)(1-5x) \right]. \quad (\text{A3})$$

The  $\mathcal{O}(\alpha_s^2)$  expression is split up into a hard-gluon and a soft-plus-virtual-gluon part. In the hard part we only keep soft-gluon radiation terms of the type  $(1-x)^{-1} \ln^i(1-x)$ . It is given by

$$\begin{aligned} & \Gamma_{qq}^{(2),H}(x, \kappa^2, R^2, M^2) \\ &= \left[ \frac{\alpha_s(R^2)}{\pi} \right]^2 C_F \left[ C_F \left\{ \frac{1}{2} \ln^3(1-x) + \frac{9}{8} \ln^2(1-x) + \left[ \frac{13}{16} + \frac{1}{2} \zeta(2) \right] \ln(1-x) + \frac{9}{32} + \frac{5}{2} \zeta(3) \right. \right. \\ & \quad \left. \left. + \left[ \ln(1-x) + \frac{3}{4} \right] \ln^2 \frac{\kappa^2}{M^2} + \left[ \frac{3}{2} \ln^2(1-x) + \frac{9}{4} \ln(1-x) + \frac{13}{16} + \zeta(2) \right] \ln \frac{\kappa^2}{M^2} \right\} \right. \\ & \quad \left. + C_A \left\{ -\frac{11}{8} \ln^2(1-x) + \left[ \frac{169}{144} - \frac{1}{2} \zeta(2) \right] \ln(1-x) + \frac{57}{32} \right. \right. \\ & \quad \left. \left. + \frac{11}{12} \zeta(2) - \frac{3}{4} \zeta(3) - \frac{11}{24} \ln^2 \frac{\kappa^2}{M^2} - \frac{11}{12} \ln \frac{M^2}{R^2} \ln \frac{\kappa^2}{M^2} \right. \right. \\ & \quad \left. \left. + \left[ -\frac{11}{6} \ln(1-x) + \frac{67}{36} - \frac{1}{2} \zeta(2) \right] \ln \frac{\kappa^2}{M^2} \right. \right. \\ & \quad \left. \left. + \left[ -\frac{11}{12} \ln(1-x) - \frac{11}{16} \right] \ln \frac{M^2}{R^2} \right\} \right. \\ & \quad \left. + n_f \left\{ \frac{1}{4} \ln^2(1-x) - \frac{11}{72} \ln(1-x) - \frac{5}{16} - \frac{1}{6} \zeta(2) \right. \right. \\ & \quad \left. \left. + \frac{1}{12} \ln^2 \frac{\kappa^2}{M^2} + \frac{1}{6} \ln \frac{M^2}{R^2} \ln \frac{\kappa^2}{M^2} + \left[ \frac{1}{3} \ln(1-x) - \frac{5}{18} \right] \ln \frac{\kappa^2}{M^2} \right. \right. \\ & \quad \left. \left. + \left[ \frac{1}{6} \ln(1-x) + \frac{1}{8} \right] \ln \frac{M^2}{R^2} \right\} \right] \frac{1}{1-x} \theta(1-x-\delta). \quad (\text{A4}) \end{aligned}$$

The soft-plus-virtual-gluon part, which is proportional to  $\delta(1-x)$ , is represented by

$$\begin{aligned} & \Gamma_{qq}^{(2),S+V}(x, \kappa^2, R^2, M^2) \\ &= \left[ \frac{\alpha_s(R^2)}{\pi} \right]^2 C_F \left[ C_F \left\{ \frac{1}{8} \ln^4 \delta + \frac{3}{8} \ln^3 \delta + \left[ \frac{13}{32} + \frac{1}{4} \zeta(2) \right] \ln^2 \delta + \left[ \frac{9}{32} + \frac{5}{2} \zeta(3) \right] \ln \delta - \frac{1}{32} - \frac{5}{16} \zeta(2) \right. \right. \\ & \quad \left. \left. + 3 \zeta(3) + \frac{59}{40} \zeta(2)^2 + \left[ \frac{1}{2} \ln^2 \delta + \frac{3}{4} \ln \delta + \frac{9}{32} - \frac{1}{2} \zeta(2) \right] \ln^2 \frac{\kappa^2}{M^2} \right. \right. \\ & \quad \left. \left. + \left[ \frac{1}{2} \ln^3 \delta + \frac{9}{8} \ln^2 \delta + \left[ \frac{13}{16} + \zeta(2) \right] \ln \delta + \frac{9}{32} + \frac{5}{2} \zeta(3) \right] \ln \frac{\kappa^2}{M^2} \right\} \right. \\ & \quad \left. + C_A \left\{ -\frac{11}{24} \ln^3 \delta + \left[ \frac{169}{288} - \frac{1}{4} \zeta(2) \right] \ln^2 \delta + \left[ \frac{57}{32} + \frac{11}{12} \zeta(2) - \frac{3}{4} \zeta(3) \right] \ln \delta + \frac{215}{288} + \frac{1049}{144} \zeta(2) \right. \right. \\ & \quad \left. \left. - \frac{49}{24} \zeta(3) - \frac{77}{80} \zeta(2)^2 + \left[ -\frac{11}{24} \ln \delta - \frac{11}{32} \right] \ln^2 \frac{\kappa^2}{M^2} + \left[ -\frac{11}{12} \ln \delta - \frac{11}{16} \right] \ln \frac{M^2}{R^2} \ln \frac{\kappa^2}{M^2} \right. \right. \\ & \quad \left. \left. + \left[ -\frac{11}{12} \ln^2 \delta + \left[ \frac{67}{36} - \frac{1}{2} \zeta(2) \right] \ln \delta + \frac{193}{96} - \frac{3}{4} \zeta(3) \right] \ln \frac{\kappa^2}{M^2} \right. \right. \\ & \quad \left. \left. + \left[ -\frac{11}{24} \ln^2 \delta - \frac{11}{16} \ln \delta - \frac{11}{48} - \frac{11}{6} \zeta(2) \right] \ln \frac{M^2}{R^2} \right\} \right] \end{aligned}$$

$$\begin{aligned}
& + n_f \left\{ \frac{1}{12} \ln^3 \delta - \frac{11}{144} \ln^2 \delta + \left[ -\frac{5}{16} - \frac{1}{6} \zeta(2) \right] \ln \delta - \frac{19}{144} - \frac{85}{72} \zeta(2) + \frac{1}{6} \zeta(3) \right. \\
& \quad + \left[ \frac{1}{12} \ln \delta + \frac{1}{16} \right] \ln^2 \frac{\kappa^2}{M^2} + \left[ \frac{1}{6} \ln \delta + \frac{1}{8} \right] \ln \frac{M^2}{R^2} \ln \frac{\kappa^2}{M^2} + \left[ \frac{1}{6} \ln^2 \delta - \frac{5}{18} \ln \delta - \frac{17}{48} \right] \ln \frac{\kappa^2}{M^2} \\
& \quad \left. + \left[ \frac{1}{12} \ln^2 \delta + \frac{1}{8} \ln \delta + \frac{1}{24} + \frac{1}{3} \zeta(2) \right] \ln \frac{M^2}{R^2} \right\} \delta(1-x), \quad (\text{A5})
\end{aligned}$$

where  $n_f$  denotes the number of light flavors.

## APPENDIX B

From the  $O(\alpha_s^2)$  splitting functions  $\Gamma_{qq}^{DC}$  in Appendix A and (3.1) we infer the  $O(\alpha_s^2)$  soft-plus-virtual-gluon approximations to reaction (2.1). Like in the case of the transition functions in Appendix A we split the cross section into a hard-gluon part where we only keep large logarithms of the type  $(s_4 - M_W^2)^{-1} \ln^i(s_4 - M_W^2)$ , given by

$$\begin{aligned}
& \left[ s^2 \frac{d\sigma_{q\bar{q}}^{(2)}}{dt du} \right]_{s_4 \rightarrow M_W^2}^H \\
& = \left[ \frac{\alpha_s(R^2)}{\pi} \right]^2 C_F \left[ C_F \left\{ \frac{1}{2} \ln^3 \frac{s_4 - M_W^2}{s+t} + \frac{1}{2} \ln^2 \frac{s_4 - M_W^2}{s+t} \ln \frac{s_4 - M_W^2}{s+u} + \frac{3}{4} \ln \frac{s_4 - M_W^2}{s+t} \ln \frac{s_4 - M_W^2}{s+u} + \frac{3}{2} \ln^2 \frac{s_4 - M_W^2}{s+t} \right. \right. \\
& \quad + \left[ \frac{13}{8} + 2\zeta(2) \right] \ln \frac{s_4 - M_W^2}{s+t} + \frac{15}{32} + \frac{3}{4} \zeta(2) + \frac{7}{2} \zeta(3) + \left[ 2 \ln \frac{s_4 - M_W^2}{s+t} + \frac{3}{2} \right] \ln^2 \frac{s}{M^2} \\
& \quad \left. + \left[ \ln \frac{s_4 - M_W^2}{s+t} \ln \frac{s_4 - M_W^2}{s+u} + 2 \ln^2 \frac{s_4 - M_W^2}{s+t} + \frac{9}{2} \ln \frac{s_4 - M_W^2}{s+t} + \frac{13}{8} + 2\zeta(2) \right] \ln \frac{s}{M^2} \right\} \\
& \quad + C_A \left\{ -\frac{11}{8} \ln^2 \frac{s_4 - M_W^2}{s+t} + \left[ \frac{169}{144} - \frac{1}{2} \zeta(2) \right] \ln \frac{s_4 - M_W^2}{s+t} + \frac{57}{32} + \frac{11}{12} \zeta(2) - \frac{3}{4} \zeta(3) - \frac{11}{24} \ln^2 \frac{s}{M^2} \right. \\
& \quad - \frac{11}{12} \ln \frac{M^2}{R^2} \ln \frac{s}{M^2} + \left[ -\frac{11}{6} \ln \frac{s_4 - M_W^2}{s+t} + \frac{67}{36} - \frac{1}{2} \zeta(2) \right] \ln \frac{s}{M^2} \\
& \quad \left. + \left[ -\frac{11}{12} \ln \frac{s_4 - M_W^2}{s+t} - \frac{11}{16} \right] \ln \frac{M^2}{R^2} \right\} \\
& \quad + n_f \left\{ \frac{1}{4} \ln^2 \frac{s_4 - M_W^2}{s+t} - \frac{11}{72} \ln \frac{s_4 - M_W^2}{s+t} - \frac{5}{16} - \frac{1}{6} \zeta(2) + \frac{1}{12} \ln^2 \frac{s}{M^2} + \frac{1}{6} \ln \frac{M^2}{R^2} \ln \frac{s}{M^2} \right. \\
& \quad \left. + \left[ \frac{1}{3} \ln \frac{s_4 - M_W^2}{s+t} - \frac{5}{18} \right] \ln \frac{s}{M^2} + \left[ \frac{1}{6} \ln \frac{s_4 - M_W^2}{s+t} + \frac{1}{8} \right] \ln \frac{M^2}{R^2} \right\} \\
& \quad \times \frac{1}{s_4 - M_W^2} \theta(s_4 - M_W^2 - \Delta) B_{\text{QED}}(s, t, u, M_W^2) + (t \leftrightarrow u, Q_1 \leftrightarrow Q_2), \quad (\text{B1})
\end{aligned}$$

and a corresponding soft-plus-virtual part proportional to  $\delta(s_4 - M_W^2)$ , namely,

$$\begin{aligned}
& \left[ s^2 \frac{d\sigma_{q\bar{q}}^{(2)}}{dt du} \right]^{S+V} \\
& = \left[ \frac{\alpha_s(R^2)}{\pi} \right]^2 C_F \left[ C_F \left\{ \frac{1}{8} \ln^2 \frac{\Delta}{s+t} \ln^2 \frac{\Delta}{s+u} + \frac{1}{8} \ln^4 \frac{\Delta}{s+t} + \frac{3}{8} \ln^2 \frac{\Delta}{s+t} \ln \frac{\Delta}{s+u} + \frac{3}{8} \ln^3 \frac{\Delta}{s+t} \right. \right. \\
& \quad + \left[ \frac{13}{16} + \zeta(2) \right] \ln^2 \frac{\Delta}{s+t} + \left[ \frac{15}{32} + \frac{3}{4} \zeta(2) + \frac{7}{2} \zeta(3) \right] \ln \frac{\Delta}{s+t} - \frac{3}{32} \zeta(2) \\
& \quad \left. + \frac{137}{40} \zeta^2(2) + \frac{15}{4} \zeta(3) + \left[ \ln^2 \frac{\Delta}{s+t} + \frac{3}{2} \ln \frac{\Delta}{s+t} + \frac{9}{16} - \zeta(2) \right] \ln^2 \frac{s}{M^2} \right\}
\end{aligned}$$

$$\begin{aligned}
& + \left[ \frac{1}{2} \ln^2 \frac{\Delta}{s+t} \ln \frac{\Delta}{s+u} + \frac{1}{2} \ln^3 \frac{\Delta}{s+t} + \frac{9}{4} \ln^2 \frac{\Delta}{s+t} \right. \\
& \quad \left. + \left[ \frac{13}{8} + 2\zeta(2) \right] \ln \frac{\Delta}{s+t} + \frac{15}{32} + \frac{3}{4} \zeta(2) + \frac{7}{2} \zeta(3) \right] \ln \frac{s}{M^2} \Bigg\} \\
& + C_A \left\{ -\frac{11}{24} \ln^3 \frac{\Delta}{s+t} + \left[ \frac{169}{288} - \frac{1}{4} \zeta(2) \right] \ln^2 \frac{\Delta}{s+t} \right. \\
& \quad + \left[ \frac{57}{32} + \frac{11}{12} \zeta(2) - \frac{3}{4} \zeta(3) \right] \ln \frac{\Delta}{s+t} + \frac{215}{288} + \frac{1049}{144} \zeta(2) - \frac{49}{24} \zeta(3) - \frac{77}{80} \zeta^2(2) \\
& \quad + \left[ -\frac{11}{24} \ln \frac{\Delta}{s+t} - \frac{11}{32} \right] \ln^2 \frac{s}{M^2} + \left[ \frac{11}{12} \ln \frac{\Delta}{s+t} - \frac{11}{16} \right] \ln \frac{M^2}{R^2} \ln \frac{s}{M^2} \\
& \quad + \left[ -\frac{11}{12} \ln^2 \frac{\Delta}{s+t} + \left[ \frac{67}{36} - \frac{1}{2} \zeta(2) \right] \ln \frac{\Delta}{s+t} + \frac{193}{96} - \frac{3}{4} \zeta(3) \right] \ln \frac{s}{M^2} \\
& \quad \left. + \left[ -\frac{11}{24} \ln^2 \frac{\Delta}{s+t} - \frac{11}{16} \ln \frac{\Delta}{s+t} - \frac{11}{48} - \frac{11}{6} \zeta(2) \right] \ln \frac{M^2}{R^2} \right\} \\
& + n_f \left\{ \frac{1}{12} \ln^3 \frac{\Delta}{s+t} - \frac{11}{144} \ln^2 \frac{\Delta}{s+t} + \left[ -\frac{5}{16} - \frac{1}{6} \zeta(2) \right] \ln \frac{\Delta}{s+t} \right. \\
& \quad - \frac{19}{144} - \frac{85}{72} \zeta(2) + \frac{1}{6} \zeta(3) + \left[ \frac{1}{12} \ln \frac{\Delta}{s+t} + \frac{1}{16} \right] \ln^2 \frac{s}{M^2} + \left[ \frac{1}{6} \ln \frac{\Delta}{s+t} + \frac{1}{8} \right] \ln \frac{M^2}{R^2} \ln \frac{s}{M^2} \\
& \quad \left. + \left[ \frac{1}{6} \ln^2 \frac{\Delta}{s+t} - \frac{5}{18} \ln \frac{\Delta}{s+t} - \frac{17}{48} \right] \ln \frac{s}{M^2} + \left[ \frac{1}{12} \ln^2 \frac{\Delta}{s+t} + \frac{1}{8} \ln \frac{\Delta}{s+t} + \frac{1}{24} + \frac{1}{3} \zeta(2) \right] \ln \frac{M^2}{R^2} \right\} \\
& \quad \times \delta(s_4 - M_W^2) B_{\text{QED}}(s, t, u, M_W^2) + (t \leftrightarrow u, Q_1 \leftrightarrow Q_2). \tag{B2}
\end{aligned}$$

- [1] J. F. Owens and W.-K. Tung, *Annu. Rev. Nucl. Part. Sci.* **42**, 291 (1992).
- [2] S. G. Gorishny, A. L. Kataev, and S. A. Larin, *Phys. Lett. B* **212**, 238 (1988); **259**, 144 (1991); L. R. Surguladze and M. A. Samuel, *Phys. Rev. Lett.* **66**, 560 (1991); **66**, 2416(E) (1991).
- [3] G. Kramer and B. Lampe, *Z. Phys. C* **34**, 497 (1987).
- [4] T. Matsuura, R. Hamburg, and W. L. van Neerven, *Nucl. Phys.* **B359**, 343 (1991).
- [5] W. L. van Neerven and E. B. Zijlstra, *Nucl. Phys.* **B382**, 11 (1992).
- [6] P. Aurenche, R. Baier, M. Fontannaz, and D. Schiff, *Nucl. Phys.* **B286**, 509 (1987); **B297**, 661 (1988); A. P. Contogouris and S. Papadopoulos, *Mod. Phys. Lett. A* **5**, 901 (1990); **5**, 1951 (1990).
- [7] P. Nason, D. Dawson, and R. K. Ellis, *Nucl. Phys.* **B303**, 607 (1988); **B327**, 49 (1989); **B335**, 260(E) (1990).
- [8] W. Beenakker, H. Kuijff, W. L. van Neerven, and J. Smith, *Phys. Rev. D* **40**, 54 (1989); W. Beenakker, W. L. van Neerven, R. Meng, G. A. Schuler, and J. Smith, *Nucl. Phys.* **B351**, 507 (1991).
- [9] J. Smith, W. L. van Neerven, and J. A. M. Vermaseren, *Z. Phys. C* **30**, 621 (1986).
- [10] J. Smith, D. Thomas, and W. L. van Neerven, *Z. Phys.* **44**, 267 (1989).
- [11] K. O. Mikaelian, *Phys. Rev. D* **17**, 750 (1978); K. O. Mikaelian, M. A. Samuel, and D. Sahdev, *Phys. Rev. Lett.* **43**, 746 (1979); R. W. Brown, D. Sadhev, and K. O. Mikaelian, *Phys. Rev. D* **20**, 1164 (1979); T. R. Grose and K. O. Mikaelian, *ibid.* **23**, 123 (1981).
- [12] G. N. Valenzuela and J. Smith, *Phys. Rev. D* **31**, 2787 (1985); J. Cortes, K. Hagiwara, and F. Herzog, *Nucl. Phys.* **B278**, 26 (1986).
- [13] U. Bauer and D. Zeppenfeld, *Nucl. Phys.* **B308**, 127 (1988).
- [14] UA2 Collaboration, J. Alitti *et al.*, *Phys. Lett. B* **277**, 194 (1992).
- [15] M. A. Samuel, G. Li, N. Sinha, R. Sinha, and M. K. Sundaresan, *Phys. Rev. Lett.* **67**, 9 (1991), *Phys. Lett. B* **280**, 124 (1992).
- [16] J. G. Morfín and W.-K. Tung, *Z. Phys. C* **52**, 13 (1991).
- [17] M. Diemoz, F. Ferroni, E. Longo, and G. Martinelli, *Z. Phys. C* **39**, 121 (1988).
- [18] J. Kuber-André and F. E. Paige, *Phys. Rev. D* **19**, 221 (1979).
- [19] G. Altarelli, R. K. Ellis, and G. Martinelli, *Nucl. Phys.* **B157**, 461 (1979).
- [20] B. Humpert and W. L. van Neerven, *Nucl. Phys.* **B184**, 1225 (1981).
- [21] R. Meng, G. A. Schuler, J. Smith, and W. L. van Neerven, *Nucl. Phys.* **B339**, 325 (1990); E. Laenen, J. Smith, and W. L. van Neerven, *Nucl. Phys.* **B369**, 543 (1992).
- [22] G. Altarelli, M. Diemoz, G. Martinelli, and P. Nason, *Nucl. Phys.* **B308**, 724 (1988).
- [23] J. Ohnemus, *Phys. Rev. D* **47**, 940 (1993).